Title: Targeting Siglec-10/α3β1 Integrin Interactions Enhances Macrophage-Mediated Phagocytosis of Pancreatic Cancer

Running Title: Role of Siglec-10 in Immune Evasion in Pancreatic Cancer

Author list: Pratima Saini[1], Gauri Mirji[2], Sajad Ahmed Bhat[2], Kar Muthumani[2#], Joel Cassel[2], Hsin-Yao Tang[2], Hiroaki Tateno[3], Rugang Zhang[4], Rahul S. Shinde[2], Mohamed Abdel-Mohsen[1†]

Affiliations: [1]Northwestern University, Chicago, IL, USA; [2]The Wistar Institute, Philadelphia, PA, USA; [3]Cellular and Molecular Biotechnology Research Institute, National Institute of Advanced Industrial Science and Technology (AIST), Tsukuba, Ibaraki, Japan; [4]University of Texas MD Anderson Cancer Center, Houston, TX, USA.

[#] Current affiliation: Merck & Co., Inc., Rahway, NJ, USA

[†]Corresponding author: Mohamed Abdel-Mohsen, Ph.D. Associate Professor, Northwestern University; Chicago, IL 60611. Phone: 312-503-4946. Email: mmohsen@northwestern.edu

ABSTRACT

Tumor-associated macrophages (TAMs) in the tumor microenvironment exhibit impaired phagocytic activity, contributing to tumor progression. Here, we identify integrin α3β1, composed of ITGA3 and ITGB1 subunits, as a sialylated glycoprotein ligand for Siglec-10, an inhibitory receptor on TAMs in pancreatic ductal adenocarcinoma (PDAC). Mechanistically, the interaction between Siglec-10 on TAMs and α3β1 on PDAC cells suppresses macrophage-mediated phagocytosis, enabling immune evasion by PDAC. Consequently, disrupting Siglec-10 interactions with monoclonal antibodies significantly enhances macrophage phagocytosis of PDAC cells in vitro. In a PDAC xenograft mouse model engrafted with human macrophages, disrupting Siglec-10 interactions reduces tumor growth and activates the PI3K/MAPK/AP-1 signaling cascades in macrophages, enhancing their phagocytic capacity. These findings suggest that the interaction between Siglec-10 and integrin α3β1 is a key mediator of immune evasion by TAMs and highlight the therapeutic potential of targeting Siglec-10/α3β1 interactions to restore macrophage phagocytic capacity.

KEYWORDS

Pancreatic ductal adenocarcinoma (PDAC); Siglec-10; Integrin α3β1; Macrophage phagocytosis; immunotherapy; Siglecs; Sialic acid; ITGA3; ITGB1.

INTRODUCTION

There is an urgent need to identify novel immunological targets to improve the survival rates of patients with Pancreatic Ductal Adenocarcinoma (PDAC). This cancer is particularly challenging, with a five-year survival rate post-diagnosis of 12% and resistance to immunotherapy (1-3). PDAC resistance to immunotherapy is thought to arise from various mechanisms within the tumor microenvironment (TME). Notably, tumor-associated macrophages (TAMs), a major immune infiltrate in the TME, contribute significantly to treatment resistance by promoting an immunosuppressive microenvironment and by lacking the ability to eliminate cancer cells through phagocytosis (4-6). Therefore, there is a growing interest in rejuvenating macrophages' capacity for phagocytosis and thus targeted destruction of PDAC cells. This has been pursued via blocking the 'do not eat me signal' conveyed by CD47 on cancer cells, however the outcomes have not always been optimal (7-10), highlighting the need for novel strategies to achieve this goal.

One promising area in stimulating TAMs' ability to phagocytose PDAC cells lies in the field of glyco-immunology. Recent advances in this emerging field have shown that glycans play a pivotal role in modulating key immunological functions during disease. This recognition that glycans significantly influence immunological functions has led to an understanding that many tumor cells exploit aberrant glycosylation patterns to evade immune responses (11). For instance, cancer cells often upregulate sialoglycans (glycans containing sialic acid) on their cell surface proteins to suppress immune surveillance (12). Sialic acid on cancer cell glycoproteins binds to Siglecs, inhibitory receptors present on various immune cells, including TAMs. This binding trigger inhibitory signaling in TAMs, diminishing their ability to phagocytose cancer cells (13-19). Thus, Siglecs on TAMs function as 'glyco-immune checkpoints,' akin to the PD1 checkpoint on $CD8^+$ T cells. Targeting the interactions between Siglecs on TAMs and sialic acid on cancer cells therefore holds significant potential for enhancing the ability of macrophages to phagocytose cancer cells, including in PDAC.

Among the various Siglec-sialic acid interactions, the binding between Siglec-10 on TAMs and sialic acid on CD24 of cancer cells is a key interaction that inhibits TAMs' ability to phagocytose ovarian and breast cancer cells. This interaction involves the sialic acid-containing ligand CD24 on cancer cells (akin to PD-L1 on cancer cells) and the sialic acid-binding receptor

Siglec-10 on TAMs (akin to PD-1 on T cells). This interaction triggers an inhibitory signal, mediated by SHP-1 and SHP-2, which inhibits macrophage-mediated phagocytosis. This interaction has been studied primarily in ovarian and breast cancers (20). In these cancers, blockade of CD24, using an antibody, enhanced the ability of TAMs to phagocytose ovarian and breast cancer cells (20), indicating that blocking the Siglec-10 interactions improved TAMs' ability to phagocytose cancer cells. However, it remains unknown whether blocking Siglec-10 interactions can reinvigorate macrophage-mediated phagocytosis against PDAC cells.

In this study, we investigate the role of Siglec-10 interactions in PDAC immune evasion from macrophage-mediated phagocytosis. Unlike ovarian and breast cancers, where CD24 is a key ligand for Siglec-10, we found that while most PDAC cells bind to Siglec-10—indicating the presence of sialic acid ligands—these cells do not predominantly express CD24. This suggests that PDAC cells engage Siglec-10 primarily through other glycoproteins. Using affinity pulldown and mass spectrometry, we identified the glycoprotein ligands of Siglec-10 on PDAC cells as the two subunits of integrin α3β1 (ITGA3 and ITGB1), which have not previously been implicated in PDAC immune evasion. We then confirmed that ITGA3 and ITGB1 contribute to PDAC cell resistance to macrophage phagocytosis using *in vitro* immune-killing assays against PDAC cells. Since we found that Siglec-10 on macrophages interacts with multiple glycoproteins on PDAC cells, we hypothesized that directly targeting Siglec-10 would be a more effective approach than targeting its ligands. To test this, we developed novel antibodies targeting Siglec-10 and evaluated their ability to enhance macrophage phagocytosis of PDAC cells. Disrupting Siglec-10 interactions using these antibodies significantly increased macrophage-mediated phagocytosis of human PDAC cells *in vitro* and reduced tumor size in a PDAC xenograft mouse model engrafted with human macrophages.

RESULTS

PDAC cells bind to Siglec-10 through sialic acid expressed on proteins other than CD24.

To investigate the potential links between Siglec-10 or CD24 expression and PDAC progression, we first analyzed TCGA data on gene expression of pancreatic adenocarcinoma (PAAD) tissues and normal tissues. Siglec-10 expression, but not CD24 expression, is significantly higher in PAAD tissues compared to normal tissues (**Fig. 1a**). Sialic acids are added to glycoproteins, such as CD24 and others, through the action of several glycan-related enzymes, including several sialyltransferases (**Fig. 1b**). We therefore examined whether the expression of these glycan-related genes is enriched in PAAD tissues. Indeed, multiple genes involved in the production of sialic acid ligands for Siglec-10 were significantly upregulated in PAAD compared to normal tissues (**Fig. 1c-d**). These findings suggest that Siglec-10–sialic acid interactions may play a role in PDAC progression.

Interactions between sialic acid-containing ligands (e.g., CD24) on cancer cells and Siglec-10 on macrophages are known to inhibit macrophage-mediated phagocytosis and blocking CD24 enhances macrophage-mediated phagocytosis against breast and ovarian cancer cells (20). To test whether blocking CD24 could enhance macrophage phagocytosis of PDAC cells, we used a blocking antibody previously shown to enhance phagocytosis in breast and ovarian cancers (20). Monocytes isolated from PBMCs of healthy donors were differentiated into macrophages (21), leading to high Siglec-10 expression (**Supplementary Fig. 1**). These macrophages were co-cultured with phRhodo-labeled human PDAC cells from several cell lines in the presence of either an isotype control or anti-CD24 antibody. The CD24 blocking antibody failed to significantly or consistently enhance macrophage phagocytosis against PDAC cells (**Fig. 1f**).

Several factors may explain why blocking CD24 did not significantly or consistently enhance macrophage phagocytosis of PDAC cells. One possibility is that PDAC cells do bind to Siglec-10 on macrophages, but they do so through sialic acid expressed on other glycoproteins, instead of or in addition to CD24. To explore this possibility, we used a recombinant Siglec-10-Fc chimera protein with a BV421-conjugated secondary antibody to detect Siglec-10 ligands via flow cytometry. Several human PDAC cell lines, including MIA PaCa-2, AsPC-1, and BxPC-3 bound Siglec-10, indicating the presence of the preferred sialic acid type on their surface glycoproteins (**Fig. 1g; x-axis**). Although some Siglec-10–binding cells did express CD24, the

majority of these cells do not express CD24 (**Fig. 1g-h**). These data indicate that PDAC cells utilize additional glycoproteins, apart from CD24, to bind Siglec-10. This contrasts with breast and ovarian cancers, where CD24 is the primary Siglec-10–binding glycoprotein (20).

Siglec-10 binds to ITGA3 and ITGB1, the subunits of α3β1 Integrin, on PDAC cells.

To identify glycoproteins on PDAC cells that bind to Siglec-10, we performed a pull-down assay using recombinant Siglec-10 and cell-membrane proteins isolated from several human PDAC cell lines. Proteins bound to Siglec-10 were identified via mass spectrometry analysis (**Fig. 2a**). From a total of 4,044 proteins whose binding was enriched compared to a no-protein control, 110 proteins showed enrichment compared to a Siglec-5 (a closely related Siglec used as a control). Of these, six proteins—CD47, CD59, CD73, ITGB6, ITGA3, and ITGB1—were significantly overexpressed in PAAD tissues compared to normal tissues based on TCGA data (**Fig. 2b**).

To determine whether these six proteins bind directly to Siglec-10, we performed surface plasmon resonance (SPR) analysis with immobilized recombinant Siglec-10 protein using recombinant versions of these proteins. Among the six candidates, only ITGA3 and ITGB1, the subunits of α3β1 integrin, exhibited strong binding affinity to Siglec-10 (**Fig. 2c**). To assess whether this binding is dependent on the sialic acid content of these glycoproteins, we treated ITGA3 and ITGB1 with sialidase to enzymatically remove sialic acid. The removal of sialic acid was confirmed using lectin staining with a sialic acid–specific lectin (SNA), which showed a significant reduction in sialic acid levels on ITGA3 and ITGB1 after sialidase treatment (**Fig. 2d**). Sialidase treatment abolished the ability of ITGA3 and ITGB1 to bind to Siglec-10 (**Fig. 2e-f**). These findings show that Siglec-10 binds to the sialic acid on ITGA3 and ITGB1.

The expression of ITGA3 and ITGB1 on PDAC cells correlates with PDAC progression and prognosis.

Having identified ITGA3 and ITGB1 as glycoprotein ligands that interact with Siglec-10 to potentially suppress immune surveillance, we next investigated whether their expression is associated with PDAC progression and prognosis. First, we measured the cell surface expression of ITGA3 and ITGB1 on several human PDAC cell lines. High levels of ITGA3 (**Fig. 3a, and**

Supplementary Fig. 2a) were observed across multiple PDAC cell lines. We then analyzed TCGA data to assess the *in vivo* relevance of ITGA3 expression in PAAD tissues compared to normal tissues. PAAD tissues exhibited significantly higher levels of ITGA3 compared to normal tissues. Similar results were observed with ITGB1 (**Fig. 3c-d, and Supplementary Fig. 2b).** ITGA3 expression correlated with elevated Siglec-10 expression (**Supplementary Fig. 3a**) and higher levels of glycan-related genes, such as ST3GAL1 and B2GNT3, responsible for sialic acid addition to glycoproteins (**Supplementary Fig. 3b**). Similarly, ITGB1 expression correlated with increased Siglec-10 expression (**Supplementary Fig. 3c**) and elevated levels of sialic acid–related genes (**Supplementary Fig. 3d**).

Next, we investigated whether the expression of CD24 (a previously identified Siglec-10 ligand), ITGA3, and ITGB1 correlated with PDAC patient survival. While CD24 expression did not correlate with survival (**Fig. 3e**), higher expression of ITGA3 (**Fig. 3f**) and ITGB1 (**Fig. 3g**) was significantly associated with worse prognosis. These findings support the concept that ITGA3 and ITGB1 contribute to PDAC progression, possibly by binding to the immune-suppressing molecule Siglec-10, potentially aiding PDAC cells in evading immune-mediated surveillance.

Finally, we examined the single-cell expression of ITGA3 and ITGB1 in epithelial cells from human PDAC tissues and healthy tissues. To do this, we utilized two publicly available single-cell transcriptomic datasets of human PDAC tissues and normal tissues (22,23). In the first dataset (22), PDAC tissues and normal tissues underwent single-cell analysis (**Fig. 3h**). The single-cell expression of ITGA3 was significantly higher in PDAC epithelial cells compared to normal epithelial cells (**Fig. 3i**). Pathway analysis of $ITGA3^{hi}$ versus $ITGA3^{low}$ PDAC cells revealed differential expression of genes related to immune modulation (**Fig. 3j**). Similarly, the single-cell expression of ITGB1 was significantly higher in PDAC epithelial cells compared to normal epithelial cells (**Fig. 3k**). Pathway analysis of $ITGB1^{hi}$ versus $ITGB1^{low}$ PDAC cells showed altered pathways associated with immune evasion and modulation (**Supplementary Fig. 4a**). The second dataset (23), while lacking samples from normal tissues (**Supplementary Fig. 4b**), provided additional evidence. Analysis of $ITGA3^{hi}$ versus $ITGA3^{low}$ PDAC epithelial cells in this dataset (**Supplementary Fig. 4c-d**) confirmed the differential expression of several cellular pathways involved in immune modulation and evasion. Together, these single-cell data

from primary PDAC tissues support the role of ITGA3 and ITGB1 in promoting PDAC progression through altered immune-modulatory pathways.

ITGA3 and ITGB1 facilitate PDAC cell evasion of macrophage-mediated phagocytosis.

Given that 1) the sialic acid on ITGA3 and ITGB1 in PDAC cells binds strongly to Siglec-10, 2) ITGA3 and ITGB1 expression is associated with PDAC progression and worse prognosis, and 3) Siglec-10 interactions on macrophages inhibit their ability to phagocytose pathological cells, we next investigated whether PDAC cells with high ITGA3 or ITGB1 expression exhibit greater evasion of macrophage-mediated phagocytosis compared to cells with low expression of these glycoproteins.

We used the PDAC cell lines MIA PaCa-2 and PANC-1 and employed antibody-coated columns targeting ITGA3 or ITGB1 (**Fig. 4a**) to enrich for ITGA3^{low} or ITGB1^{low} cells, which are the cells that do not bind to the columns. Flow cytometry confirmed a significant enrichment of ITGA3^{low} and ITGB1^{low} cells compared to controls, which consisted largely of ITGA3^{hi} or ITGB1^{hi} cells that passed through the columns without being captured. **Figure 4b** illustrates an example where depleting MIA PaCa-2 cells from ITGA3^{hi} cells resulted in over a 70% reduction of ITGA3 expression. Notably, ITGA3^{low} cells showed a significant (>70%) reduction in Siglec-10 ligand expression, suggesting that they have a decreased capacity to bind Siglec-10 on macrophages and, therefore, a reduced ability to evade immune surveillance (**Fig. 4b**). Consistent with this observation, when we assessed the ability of PDAC cells with high (control) or low levels of ITGA3 to evade macrophage-mediated phagocytosis in our previously described assay (**Fig. 4c**), cells with high ITGA3 expression evaded phagocytosis significantly more effectively than ITGA3^{low} cells (**Fig. 4d-e**). Similarly, PDAC cells with high ITGB1 levels also demonstrated greater evasion of macrophage-mediated phagocytosis compared to ITGB1^{low} cells (**Fig. 4f–i**). These findings indicate that ITGA3 and ITGB1 significantly contribute to the immune evasion of PDAC cells by inhibiting macrophage-mediated phagocytosis, potentially through their interactions with Siglec-10.

Disrupting Siglec-10 interactions, via monoclonal antibodies, enhances macrophage-mediated phagocytosis of PDAC cells in vitro.

Our findings thus far suggest that Siglec-10 on macrophages binds to multiple glycoprotein ligands on PDAC cells, including ITGA3, ITGB1, and potentially others. This binding inhibits the phagocytic capacity of macrophages against PDAC cells (**Fig. 5a**). Therefore, directly targeting Siglec-10 itself, rather than its individual ligands, may be necessary to enhance macrophage-mediated phagocytosis of PDAC cells. Such an approach would disrupt interactions between Siglec-10 and sialic acids across its various glycoprotein ligands. However, the lack of potent, commercially available anti-Siglec-10 antibodies has necessitated the development of these antibodies in-house.

To generate mAbs targeting Siglec 10, mice were immunized with recombinant human Siglec-10 protein, and serum antibody titers were measured using indirect ELISA. High reactivity to Siglec-10 was observed in several mice, which were subsequently selected for hybridoma generation. Over 200 hybridoma clones were initially screened for antibody production using binding specificities by ELISA against Siglec-10 and Siglec-5 (a control). Sixteen clones (sequences in **supplementary Table 1**) were selected for subcloning. Antibodies from these clones were further characterized by ELISA and flow cytometry-based immune assays. Several antibodies exhibited high affinity for Siglec-10 in binding ELISA (**Fig. 5b**). In addition, FACS confirmed the binding specificity of these antibodies to Siglec-10: CHO-K1 cells expressing Siglec-10 or Siglec-5 (as a control) were incubated with hybridoma supernatants and stained with an Alexa Fluor 488-conjugated secondary antibody. The antibodies showed significant binding to Siglec-10-expressing cells, but not to Siglec-5 controls (**Fig. 5c**), confirming their specificity.

The clones were then evaluated for their ability to enhance macrophage-mediated phagocytosis of PDAC cells (**Fig. 5d**) using the same assay described in Fig. 1e and compared against an isotype control, an aCD24 antibody, and a commercially available aSiglec-10 antibody. Several of these clones significantly enhanced the macrophages' ability to phagocytose PDAC cells (**Fig. 5d)**. The top five clones were further tested for their ability to enhance macrophage-mediated phagocytosis of PDAC cells using macrophages derived from the monocytes of several donors.

One clone, 68A11A1, demonstrated superior performance and was selected for recombinant expression (**Fig. 5e-f**). The recombinant 68A11A1 antibody displayed high specificity for Siglec-10 without cross-reactivity to Siglec-5 or other irrelevant His-tagged proteins (**Fig. 5g**). Notably, this recombinant antibody significantly enhanced the phagocytic capacity of macrophages against multiple human PDAC cell lines compared to the antibody targeting CD24, using a similar assay as shown in Fig. 1e and using macrophages from multiple donors (**Fig. 5h**). Together, these results show the successful generation and characterization of monoclonal antibodies with high affinity and specificity for Siglec-10. These antibodies enhanced macrophage-mediated phagocytosis of PDAC cells, further underscoring the critical role of Siglec-10 interactions in immune evasion by PDAC cells and their potential as therapeutic targets.

Disrupting Siglec-10 interactions enhances macrophage-mediated phagocytosis of PDAC cells and induces human macrophage activation in vivo.

Since mice lack Siglec-10 and instead express a homolog, testing a Siglec-10 antibody in wild-type mice is not feasible. To address this, we utilized immunodeficient NSG mice engrafted with AsPC-1 human PDAC cells and human monocyte-derived macrophages. Mice were treated with either an isotype control antibody or the Siglec-10-specific antibody, clone 68A11A1 (**Fig. 6a**). Targeting Siglec-10 significantly reduced PDAC tumor growth *in vivo* (**Fig. 6b-e**).

At the end of the experiment, tumors were collected, and human macrophages were isolated using FACS (**Supplementary Fig. 5**). Transcriptomic analysis of isolated macrophages by RNA-sequencing showed significant changes in gene expression, supporting the impact of disrupting Siglec-10 interactions on macrophage activation and enhanced phagocytic capacity (**Fig. 6f-h)**. In particular, macrophages from mice treated with the Siglec-10 antibody displayed significant activation of PI3K/AKT, MAPK, and AP-1 immune signaling pathways; all key pathway downstream of Siglec-10 interactions. Upregulated genes included PIK3C2A, PTEN, and PRKAA1, which regulate PI3K/AKT signaling critical for macrophage survival, metabolic reprogramming, and phagocytosis. Genes such as MAP3K1, MAP3K2, and DUSP1 modulate MAPK signaling, and their up-regulation support balanced activation and feedback inhibition for sustained immune responses. JUN and FOS, components of the AP-1 transcription complex,

were upregulated, which can support immune responses. Additional upregulated genes such as NFKBIZ indicated induced immune activation. Conversely, downregulation of MAP2K2, CREB3, and PPP2R1A suggested a shift in MAPK signaling toward activation of JNK and p38 branches, favoring immune activation over ERK-mediated proliferation. Reduced expression of MIF, an immune regulator, further alleviated inhibitory effects on macrophage activation (**Fig. 6f)**.

In addition, macrophages from mice treated with the Siglec-10 antibody showed up-regulation of several pathways related to enhanced phagocytosis. Up-regulated genes including RAB5A, which controls phagosome maturation and vesicle trafficking; DOCK1, which activates Rac1 to drive actin remodeling essential for phagocytic cup formation; and CDC42EP3, which facilitates actin filament organization. Other upregulated genes included CD46, a complement receptor linking target recognition to enhanced phagocytosis; WASL, which promotes actin polymerization crucial for stabilizing the phagocytic cup; PLXNB1, which modulates cytoskeletal changes; and ACTN4, ARHGAP12, and ROCK2, which regulate actin dynamics and cytoskeletal rearrangement for efficient engulfment of targets. Notably, genes such as FCGR2B and CFL1, which inhibit phagocytosis and actin remodeling, were downregulated, lifting constraints on macrophage function. These changes collectively indicate enhanced phagocytosis driven by improved actin remodeling, vesicle trafficking, and target recognition while reducing inhibitory signals (**Fig. 6g)**.

Finally, macrophages from mice treated with Siglec-10 antibody showed evidence of metabolic reprogramming. Upregulation of ACADM, PDK4, and PRKAA1 indicated a shift toward fatty acid β-oxidation, a metabolic adaptation that provides energy for sustained macrophage activation and phagocytosis. Notably, downregulation of ALDOA, a glycolytic enzyme, suggested a decreased reliance on glycolysis in favor of oxidative metabolism, aligning with the energy demands of prolonged immune responses (**Fig. 6h)**. Together, these findings show that disrupting Siglec-10 interactions enhances macrophage-mediated phagocytosis of PDAC cells *in vivo*, accompanied by extensive macrophage activation characterized by cytoskeletal remodeling, immune pathway activation, and metabolic reprogramming. These data establish targeting Siglec-10 interactions as a promising therapeutic target for immunotherapy in PDAC.

DISCUSSION

In this study, we identified a novel immunological interaction between α3β1 integrin on PDAC cell surfaces and Siglec-10, a glyco-immune checkpoint receptor on macrophages, which facilitates immune evasion by PDAC cells. This previously unrecognized interaction suppresses macrophage-mediated immune surveillance, enabling tumor cells to evade immune clearance. Notably, we show that disrupting these interactions with monoclonal antibodies restores macrophage phagocytic capacity against PDAC cells. By tapping into glycan-based interventions, a largely underexplored avenue in cancer immunotherapy, our findings lay the foundation for innovative strategies that could enhance therapeutic outcomes for PDAC patients. With PDAC projected to account for approximately 66,440 new cases and 51,750 deaths in the United States in 2024 alone (2), this work addresses an urgent and critical clinical need.

In 2019, a pivotal study identified interactions between Siglec-10 and CD24 as a key 'don't eat me' signal in breast and ovarian cancers, mediating immune evasion through macrophage suppression (20). Our findings uncover a distinct mechanism in PDAC, where α3β1 integrin, rather than CD24, emerges as a primary ligand for Siglec-10. These findings suggest that Siglec-10 interacts with multiple ligands on cancer cell surfaces, with these ligands varying across cancer types. Such diversity highlights the critical need to identify cancer-specific Siglec-10 ligands. Identifying these ligands provides novel insights into how distinct cancers evade immune surveillance and could inform the development of therapeutics targeting both Siglec-10 and its ligands. This approach holds significant potential to enhance the efficacy of tailored immunotherapeutic strategies in oncology.

Integrin α3β1, composed of the ITGA3 and ITGB1 subunits, is a well-characterized cell surface receptor known for its roles in cell adhesion, migration, and signaling. α3β1 has been implicated in tumor progression, metastasis, and resistance to therapy across various cancer types (24-29). In PDAC, ITGA3 and ITGB1 are frequently overexpressed and contribute to the disease's aggressive nature by promoting epithelial-mesenchymal transition, invasion, and survival within the dense, immunosuppressive tumor microenvironment (30-36). However, their involvement in immune evasion has remained unexplored. In this study, we identify a previously uncharacterized function for α3β1 integrin, via its glycosylation, as a critical ligand for Siglec-10 on macrophages in PDAC. By interacting with Siglec-10, α3β1 transmits a ‘don’t eat me’ signal,

suppressing macrophage-mediated phagocytosis and facilitating immune evasion and tumor progression. These findings broaden the understanding of α3β1, extending its role beyond tumor cell behavior to include a pivotal function in immune suppression. By uncovering this mechanism of immune evasion, we highlight α3β1-Siglec-10 interactions as a promising therapeutic target to overcome immune resistance and improve outcomes for PDAC patients.

Current immunotherapy efforts focusing on targeting proteins and nucleic acids have revolutionized cancer treatment. However, these approaches remain insufficient to fully realize the potential of immunotherapy for many patients, including those with PDAC (37,38). Targeting glycomic interactions between glycans and glyco-immune checkpoints such as Siglec-10 represents a novel and complementary approach to enhance the efficacy of cancer immunotherapy (39-42). Our findings underscore the therapeutic promise of disrupting Siglec-10 interactions as a strategy to restore macrophage function and enhance anti-PDAC immunity. Unlike traditional immune checkpoint inhibitors, such as those targeting PD-1/PD-L1 interactions that primarily act on T cells, Siglec-10 targeting directly reactivates myeloid cells like macrophages, which play a pivotal role within the tumor microenvironment. This creates opportunities for combining Siglec-10 targeting with other therapies. For instance, combining it with therapies targeting immune checkpoints on T cells could further enhance anti-tumor immunity. Additionally, Siglec-10 targeting can be integrated with therapies designed to enhance macrophage-mediated phagocytosis, such as CD47-blocking antibodies, which are already in clinical development. CD47 inhibits phagocytosis by interacting with macrophage SIRPα (7,9,10). Since Siglec-10 and CD47 regulate phagocytosis through distinct pathways, targeting both simultaneously could produce additive or synergistic effects. Together, Siglec-targeting therapies, when combined with immune checkpoint inhibitors acting on T cells or macrophages, have the potential to significantly expand the arsenal of immunotherapeutic tools available for cancer treatment.

In our study, monoclonal antibodies against Siglec-10 restored macrophage phagocytic capacity *in vitro* and reduced tumor growth *in vivo*, providing a proof of concept for targeting this glyco-immune checkpoint. However, targeting Siglecs on myeloid cells could have broader implications for immunity by activating antigen-presenting cells, potentially enhancing downstream T cell responses, indirectly (43-45). In our experiments using NSG mouse models

engrafted with macrophages, we focused on the role of Siglec-10 interactions in modulating phagocytosis. However, the broader impact of disrupting these interactions on overall anti-tumor immunity warrants further investigation in models with an intact immune system such as humanized mouse models. Importantly, Siglec-sialic acid interactions serve as critical immune checkpoints to prevent autoimmunity (46). As such, blocking Siglecs may pose a risk of inducing non-specific inflammation, similar to what has been observed with other immune checkpoint inhibitors, such as PD-1/PD-L1 blockers (47). Notably, there are key differences between Siglecs and other immune checkpoints, including their expression patterns and functions. For example, a recent clinical trial (NCT03822208) evaluating a Siglec-3 (CD33) inhibitor reported favorable safety profiles in humans, suggesting that Siglec-targeted therapies may be well-tolerated. Nevertheless, careful evaluation of the balance between the beneficial and potentially detrimental effects of Siglec blockade is essential. If toxicity is observed when blocking Siglecs using monospecific antibodies, alternative approaches may be required. Bispecific or trispecific antibodies targeting both Siglec-10 and its ligands, such as the α3β1 integrin identified in this study, could represent a promising strategy. Such approaches could enhance immune responses by disrupting Siglec-10-mediated immune suppression while minimizing the risk of non-specific inflammatory effects.

While our study provides significant insights into the role of Siglec-10 interactions in PDAC immune evasion, it is not without limitations. First, our *in vivo* experiments were conducted in NSG mouse models engrafted with human macrophages, which, although useful for studying macrophage-specific effects, lack a fully intact immune system. This limits our ability to evaluate the broader impact of Siglec-10 blockade on other immune cell types, such as T cells. Second, while we identified α3β1 integrin as a critical ligand for Siglec-10 in PDAC, it is likely that additional ligands exist in other cancer types, and these remain to be explored. Third, potential off-target effects and long-term consequences of Siglec-10 blockade, such as non-specific inflammation or autoimmunity, require further investigation in more complex and clinically relevant models. Despite these limitations, our findings represent a substantial advancement in understanding glyco-immune interactions in PDAC biology. By identifying α3β1 integrin as a novel ligand for Siglec-10 and demonstrating the therapeutic potential of disrupting this interaction, we provide a new framework for targeting immune evasion in PDAC.

METHODS

Macrophage differentiation and in vitro phagocytic assay. Macrophages were differentiated as described previously (20,21). Briefly, monocytes from healthy donors were differentiated into macrophages by culturing them for 7–9 days in Iscove's Modified Dulbecco's Medium (IMDM) supplemented with 10% AB human serum (Life Technologies). During the initial 3–4 days, macrophages were stimulated with 50 ng/mL M-CSF. Subsequently, M-CSF (50 ng/ml) and IL-4 (20 ng/mL) were added to support differentiation, and this stimulation was maintained until the macrophages were used on Days 7–9. PDAC cells were treated with TrypLE Express and labeled with pHrodo Red, SE (Thermo Fisher Scientific) according to the manufacturer's protocol. Labeling was performed at a concentration of 250 ng/mL in PBS for 10 minutes at 37°C, followed by two washes with Dulbecco's Modified Eagle Medium (DMEM) containing 10% FBS and 100 U/mL penicillin/streptomycin. Healthy donor-derived macrophages were harvested using TrypLE Express, and 50,000 macrophages were seeded into black 96-well flat-bottom plates, allowing them to adhere for 30 minutes at 37°C. After adhesion, 50,000 pHrodo Red-labeled PDAC cells were added in serum-free IMDM. The plates were incubated at 37°C, and phagocytosis was monitored by imaging every hour using an Incucyte (Sartorius). The initial image (t = 0) was captured within 30 minutes of co-culture. Phagocytosis was quantified by measuring the total red area (μm^2) across technical replicates for each donor. Thresholds for identifying pHrodo Red-positive events were determined based on intensity measurements from labeled cells in the absence of macrophages.

Siglec-10 ligand staining by flow cytometry. Siglec-10 ligand expression was detected using recombinant chimeric proteins consisting of the Siglec-10 binding region fused to human IgG Fc domains (Siglec10-Fc, R&D Systems). To form the Siglec-10-Fc/anti-human IgG-BV421 complex, Siglec-10-Fc (2.5 μg/mL) and BV421-conjugated anti-human IgG were incubated on ice for 1 hour. PDAC cells were detached using TrypLE Express, washed, pelleted, and adjusted to a density of $1 \times 10^{\square}$ cells/mL. The cells were resuspended in the Siglec-10-Fc/anti-human IgG-BV421 precomplex solution along with CD24-Alexa 488 antibody. After a 30-minute incubation on ice, the cells were pelleted by centrifugation at 300 × g for 5 minutes and washed twice. Samples were analyzed using a BD FACS Symphony A3 cytometer. Data analysis was performed using FlowJo V9.

Pull-Down and mass spectrometry analysis of Siglec-10 ligands on PDAC cells. To identify Siglec-10 ligands, we employed a proximity labeling approach based on the tyramide radicalization principle (48). Briefly, recombinant Siglec-10-Fc fusion protein (10 μg) was incubated with an anti-human Fc HRP conjugate (5 μg)—a monoclonal antibody against human Fc tag directly conjugated to horseradish peroxidase (HRP)—on ice for 60 minutes to facilitate complex formation. PDAC cell lines (AsPC-1, BxPC-3, MiaPaCa-2, Panc-1) were incubated with the Siglec-10-HRP complex on ice for 1 hour (20 × 10□ cells per reaction). After incubation, cells were washed twice with 10 mL of 140 mM NaCl in 20 mM Tris-HCl buffer (pH 8.0, TBS). The cells were then treated with 10 μM biotin tyramide and 10 mM H□O□ in TBS at room temperature for 10 minutes. Following the reaction, cells were washed three times with TBS and lysed in 200 μL of lysis buffer (50 mM Tris-HCl, pH 8.0, 150 mM NaCl, 1% Nonidet P-40, 0.5% sodium deoxycholate, 0.1% SDS) supplemented with a protease inhibitor cocktail. Lysis was performed on ice for 30 minutes. A Siglec-5 control and a secondary antibody-only control were included for each cell line. The lysates were cleared by centrifugation at 15,000 × g for 30 minutes and used for the purification of biotinylated proteins.

Biotinylated proteins were purified using streptavidin-functionalized paramagnetic beads. One milligram of Dynabeads Streptavidin-MyOne C1 (Thermo Fisher Scientific) was mixed with 100 μL of cleared lysate and incubated at room temperature for 1 hour with constant shaking. The beads were collected using a magnet (DynaMag-2, Thermo Fisher Scientific) and washed extensively with D-PBS containing 0.1% SDS. The samples were reduced with tris(2-carboxyethyl)phosphine, alkylated with iodoacetamide, and digested on-bead with trypsin (Promega). Tryptic digests were cleaned using BioPureSPN C18 spin columns (Nest Group) and analyzed by liquid chromatography-tandem mass spectrometry (LC-MS/MS) using a 1.5-hour LC gradient on a Thermo Q Exactive Plus mass spectrometer (49). MS data were searched with full tryptic specificity against the UniProt human proteome (downloaded on 8/21/2023) and a contaminant database using MaxQuant 2.4.7.0 (50). Protein and peptide false discovery rates were set at 1%. A total of 4,044 proteins were identified, which were further filtered based on a two-fold enrichment of Siglec-10 compared to the Siglec-5 control.

Surface Plasmon Resonance (SPR): Recombinant Siglec-10 Fc protein was immobilized on a protein A/G chip at three different densities (~200 RU, ~600 RU, ~1000 RU). One flow cell was

left blank as a control to account for non-specific binding to the chip. All test proteins were desalted in running buffer and tested at two concentrations (100 nM and 1000 nM), except for ITGA3, which was tested at 30 nM and 300 nM. The association time was set to 120 seconds, the dissociation time to 600 seconds, and the flow rate to 25 μL/min. After each injection of test protein, the Siglec-10/protein complex was dissociated from the chip using 20 mM glycine (pH 2.0), followed by the re-immobilization of fresh Siglec-10 protein.

Sialidase treatment and lectin staining. Proteins were treated with Sialidase A (Agilent) following the manufacturer's instructions. Briefly, 5 μg of ITGA3 and ITGB1 glycoproteins were combined with 14 μL of deionized water, 4 μL of 5× Reaction Buffer, and 2 μL of Sialidase A. The reaction mixture was incubated at 37°C for 1 hour. To verify the removal of sialic acid, a lectin microarray platform was used to profile sialic acid-dependent glycan structures. This array utilizes a panel of immobilized lectins, each with known glycan structure binding specificity. Both sialidase-digested and undigested proteins were labeled with Cy3 dye (Sigma-Aldrich) and hybridized to the lectin microarray. The lectin chips were scanned for fluorescence intensity at each lectin-coated spot using an evanescent-field fluorescence scanner (Rexxam Co., Ltd.). All samples were run in triplicate, and the average fluorescence intensity of the triplicates was used for analysis. Data were normalized using the global normalization method.

ITGA3^{low} and ITGB1^{low} PDAC cell enrichment. PDAC cells were incubated with anti-human ITGA3 and ITGB1 antibodies (Clone ASC-1 and TS2/16, respectively, from Thermo Fisher Scientific) at a concentration of 1 μg/mL in 1× PBS at 4°C for 15 minutes. The cells were then washed twice and incubated with 20 μL of anti-mouse MicroBeads (Miltenyi Biotec, Cat# 130-048-402) for 15 minutes at 4°C. Following another wash, the cells were loaded onto pre-equilibrated LS columns (Miltenyi Biotec, Cat# 130-042-401) in accordance with the manufacturer's protocol. After extensive washing, the cells in the eluate fraction were pelleted, resuspended in DMEM supplemented with 10% FBS, and subsequently used for in vitro cell-killing assays.

Single-Cell RNA-Seq analysis: We analyzed two publicly available single-cell transcriptomic datasets of human PDAC and normal tissues (22,23). Data analysis was performed using BBrowser 3, with the Talk2Data plugin utilized for deeper insights. The datasets were initially categorized into PDAC and normal tissue groups. ITGA3 and ITGB1 expression in epithelial

cells was assessed, with gating performed on the PDAC cluster to separate cells based on high and low ITGA3 expression. Pathway analysis was subsequently conducted using BBrowser to identify biological processes associated with ITGA3 expression.

Siglec-10 monoclonal antibody production. Monoclonal antibodies targeting the extracellular domain (ECD) of Siglec-10 were developed and characterized. Ten BALB/c and C57BL/6 mice were initially immunized with 50μg of recombinant Siglec-10 protein (GenScript), followed by four booster immunizations of 25μg each at two-week intervals. Blood samples were collected after each immunization, and serum antibody titers were assessed using indirect ELISA. For ELISA, 96-well plates were coated with Siglec-10 antigen or Siglec-5 antigen (1μg/mL in PBS) and incubated overnight at 4°C. Plates were blocked with 1% BSA in PBS to prevent nonspecific binding. Diluted serum samples were incubated for 1 hour at 37°C, followed by washes and incubation with horseradish peroxidase (HRP)-conjugated goat anti-mouse IgG secondary antibody. The reaction was developed using tetramethylbenzidine (TMB) substrate, stopped with acid, and the absorbance was measured at 450 nm. Mice with serum OD450 values exceeding 1.0 at dilutions ≥1:8,000 were selected for hybridoma generation. Splenocytes from selected mice were fused with SP2/0 myeloma cells via electrofusion. The hybridomas were cultured in HAT medium, and supernatants were screened for Siglec-10-specific antibodies using same ELISA protocol described above. Hybridoma clones were also tested for specificity by flow cytometry (FACS) using CHO-K1 cells expressing Siglec-10 or Siglec-5 (as a control). Positive hybridoma supernatants demonstrated significant fluorescence with Siglec-10-expressing cells compared to controls. For FACS, 50 μL of a CHO-K1 cell suspension (1 × 10□ cells per well) was incubated with hybridoma supernatants at 4°C for 30 minutes. After washing, Alexa Fluor 488-conjugated goat anti-mouse IgG secondary antibody (Jackson ImmunoResearch) was added, and samples were analyzed using a flow cytometer. Clones with high median fluorescence intensity (MFI) against Siglec-10 cells were selected for subcloning.

Selected hybridoma clones underwent limiting dilution for subcloning. Subclones were cultured, and supernatants were collected for antibody purification. Antibodies were purified using Protein A chromatography and assessed for purity by SDS-PAGE. Concentrations were determined using UV spectrophotometry. The specificity of purified antibodies was validated using the same ELISA and FACS protocols described above against both Siglec-10 and Siglec-5 (as a control).

Antibodies from positive clones were sequenced. RNA was extracted from hybridoma cells using the RNeasy Isolation Kit, and antibody sequences were determined via RT-PCR using universal primers. Sequenced antibodies were expressed recombinantly in CHO-S cells and purified. Functional characterization of these recombinant antibodies was performed using the same ELISA and FACS assays described above.

In vivo mice experiments. NSG (NOD.Cg-Prkdc^{scid} Il2rg^{tm1Wjl}/SzJ) mice were anesthetized with isoflurane, and the hair on the right flank was shaved. A 100 µL suspension of AsPC-1 cells (2 × 10□ cells per mouse) was prepared by mixing the cells with Matrigel and 1× PBS at a 1:1 ratio, which was then injected subcutaneously into each mouse. After one-week, subcutaneous tumors of approximately 40 mm^3 had developed. The mice were randomly assigned to two groups: isotype control or Siglec-10 antibody treatment. Monocyte-derived macrophages were incubated with 200 µg of either isotype or Siglec-10 antibody for 30 minutes. Each mouse received intravenous injections of antibody-incubated macrophages three times per week for three weeks. Tumor size was measured using a vernier caliper, and tumor volume was calculated using the formula: tumor volume = ½ (length × width^2). All mice were maintained inappropriate environmental conditions. All animal protocols were approved by Wistar Institutional Animal Care and Use Committee (protocol # 201363). Euthanasia was performed using carbon dioxide (CO2) delivered as bottled gas, which is listed among the acceptable agents for euthanasia of laboratory rodents in the American Veterinary Medical Association (AVMA) Guidelines for the Euthanasia of Animals: 2013 Edition.

RNA-Seq analysis of macrophages. Subcutaneous tumors were excised from each mouse, and human cells were sorted by FACS. Total RNA was extracted from the sorted human macrophages using the Single Cell RNA Purification Kit (Norgen). RNA quality was assessed using the TapeStation High Sensitivity RNA ScreenTape (Agilent). Libraries were prepared using the Low Input RNA Library Prep Kit (Takara Biosciences) with 500 ng of DNase I-treated total RNA. Final library quality control was performed using the Bioanalyzer High Sensitivity DNA Kit (Agilent). Next-generation sequencing (NGS) was conducted with 100 bp paired-end reads on a NovaSeq 6000 system (Illumina) using the SP v1.5 200-cycle kit. RNA-seq analysis was performed by Bencos Research Solutions Pvt. Ltd. (Mumbai) using their proprietary TWINE BI platform. For the analysis, the RNA-seq data were aligned to the hg19 human

genome using STAR-aligner (v 2.7.10a), and salmon (v 1.10.1) was used to estimate read counts and RPKM values. Raw counts were analyzed for differential expression using DESeq2.

REFERENCES

1. Siegel RL, Miller KD, Jemal A. Cancer statistics, 2020. CA Cancer J Clin **2020**;70(1):7-30 doi 10.3322/caac.21590.

2. Siegel RL, Miller KD, Wagle NS, Jemal A. Cancer statistics, 2023. CA Cancer J Clin **2023**;73(1):17-48 doi 10.3322/caac.21763.

3. Timmer FEF, Geboers B, Nieuwenhuizen S, Dijkstra M, Schouten EAC, Puijk RS, *et al.* Pancreatic Cancer and Immunotherapy: A Clinical Overview. Cancers (Basel) **2021**;13(16) doi 10.3390/cancers13164138.

4. Beatty GL, Eghbali S, Kim R. Deploying Immunotherapy in Pancreatic Cancer: Defining Mechanisms of Response and Resistance. Am Soc Clin Oncol Educ Book **2017**;37:267-78 doi 10.1200/EDBK_175232.

5. Clark CE, Hingorani SR, Mick R, Combs C, Tuveson DA, Vonderheide RH. Dynamics of the immune reaction to pancreatic cancer from inception to invasion. Cancer Res **2007**;67(19):9518-27 doi 10.1158/0008-5472.CAN-07-0175.

6. Helm O, Held-Feindt J, Grage-Griebenow E, Reiling N, Ungefroren H, Vogel I, *et al.* Tumor-associated macrophages exhibit pro- and anti-inflammatory properties by which they impact on pancreatic tumorigenesis. Int J Cancer **2014**;135(4):843-61 doi 10.1002/ijc.28736.

7. Matlung HL, Szilagyi K, Barclay NA, van den Berg TK. The CD47-SIRPalpha signaling axis as an innate immune checkpoint in cancer. Immunol Rev **2017**;276(1):145-64 doi 10.1111/imr.12527.

8. Veillette A, Chen J. SIRPalpha-CD47 Immune Checkpoint Blockade in Anticancer Therapy. Trends Immunol **2018**;39(3):173-84 doi 10.1016/j.it.2017.12.005.

9. Weiskopf K, Jahchan NS, Schnorr PJ, Cristea S, Ring AM, Maute RL, *et al.* CD47-blocking immunotherapies stimulate macrophage-mediated destruction of small-cell lung cancer. J Clin Invest **2016**;126(7):2610-20 doi 10.1172/JCI81603.

10. Willingham SB, Volkmer JP, Gentles AJ, Sahoo D, Dalerba P, Mitra SS, *et al.* The CD47-signal regulatory protein alpha (SIRPa) interaction is a therapeutic target for human solid tumors. Proc Natl Acad Sci U S A **2012**;109(17):6662-7 doi 10.1073/pnas.1121623109.

11. RodrIguez E, Schetters STT, van Kooyk Y. The tumour glyco-code as a novel immune checkpoint for immunotherapy. Nat Rev Immunol **2018**;18(3):204-11 doi 10.1038/nri.2018.3.

12. Rodrigues E, Macauley MS. Hypersialylation in Cancer: Modulation of Inflammation and Therapeutic Opportunities. Cancers (Basel) **2018**;10(6) doi 10.3390/cancers10060207.

13. Gu Y, Zhou G, Tang X, Shen F, Ding J, Hua K. The biological roles of CD24 in ovarian cancer: old story, but new tales. Front Immunol **2023**;14:1183285 doi 10.3389/fimmu.2023.1183285.

14. Laubli H, Nalle SC, Maslyar D. Targeting the Siglec-Sialic Acid Immune Axis in Cancer: Current and Future Approaches. Cancer Immunol Res **2022**;10(12):1423-32 doi 10.1158/2326-6066.CIR-22-0366.

15. Marciel MP, Haldar B, Hwang J, Bhalerao N, Bellis SL. Role of tumor cell sialylation in pancreatic cancer progression. Adv Cancer Res **2023**;157:123-55 doi 10.1016/bs.acr.2022.07.003.

16. Saini P, Adeniji OS, Abdel-Mohsen M. Inhibitory Siglec-sialic acid interactions in balancing immunological activation and tolerance during viral infections. EBioMedicine **2022**;86:104354 doi 10.1016/j.ebiom.2022.104354.

17. Stanczak MA, Laubli H. Siglec receptors as new immune checkpoints in cancer. Mol Aspects Med **2023**;90:101112 doi 10.1016/j.mam.2022.101112.

18. Yu Y, Peng W. Recent progress in targeting the sialylated glycan-SIGLEC axis in cancer immunotherapy. Cancer Biol Med **2023**;20(5):369-84 doi 10.20892/j.issn.2095-3941.2023.0046.

19. Zhou X, Chi K, Zhang C, Liu Q, Yang G. Sialylation: A Cloak for Tumors to Trick the Immune System in the Microenvironment. Biology (Basel) **2023**;12(6) doi 10.3390/biology12060832.

20. Barkal AA, Brewer RE, Markovic M, Kowarsky M, Barkal SA, Zaro BW, *et al.* CD24 signalling through macrophage Siglec-10 is a target for cancer immunotherapy. Nature **2019**;572(7769):392-6 doi 10.1038/s41586-019-1456-0.

21. Martinez FO. Analysis of gene expression and gene silencing in human macrophages. Curr Protoc Immunol **2012**;Chapter 14:14 28 1-14 28 3 doi 10.1002/0471142735.im1428s96.

22. Peng J, Sun BF, Chen CY, Zhou JY, Chen YS, Chen H, *et al.* Single-cell RNA-seq highlights intra-tumoral heterogeneity and malignant progression in pancreatic ductal adenocarcinoma. Cell Res **2019**;29(9):725-38 doi 10.1038/s41422-019-0195-y.

23. Werba G, Weissinger D, Kawaler EA, Zhao E, Kalfakakou D, Dhara S, *et al.* Single-cell RNA sequencing reveals the effects of chemotherapy on human pancreatic adenocarcinoma and its tumor microenvironment. Nat Commun **2023**;14(1):797 doi 10.1038/s41467-023-36296-4.

24. Ganguly K, Cox JL, Ghersi D, Grandgenett PM, Hollingsworth MA, Jain M, *et al.* Mucin 5AC-Mediated CD44/ITGB1 Clustering Mobilizes Adipose-Derived Mesenchymal Stem Cells to Modulate Pancreatic Cancer Stromal Heterogeneity. Gastroenterology **2022**;162(7):2032-46 e12 doi 10.1053/j.gastro.2022.02.032.

25. Li R, Ji Q, Fu S, Gu J, Liu D, Wang L, *et al.* ITGA3 promotes pancreatic cancer progression through HIF1alpha- and c-Myc-driven glycolysis in a collagen I-dependent autocrine manner. Cancer Gene Ther **2024** doi 10.1038/s41417-024-00864-7.

26. Miskin RP, Warren JSA, Ndoye A, Wu L, Lamar JM, DiPersio CM. Integrin alpha3beta1 Promotes Invasive and Metastatic Properties of Breast Cancer Cells through Induction of the Brn-2 Transcription Factor. Cancers (Basel) **2021**;13(3) doi 10.3390/cancers13030480.

27. Subbaram S, Dipersio CM. Integrin alpha3beta1 as a breast cancer target. Expert Opin Ther Targets **2011**;15(10):1197-210 doi 10.1517/14728222.2011.609557.

28. Subbaram S, Lyons SP, Svenson KB, Hammond SL, McCabe LG, Chittur SV, *et al.* Integrin alpha3beta1 controls mRNA splicing that determines Cox-2 mRNA stability in breast cancer cells. J Cell Sci **2014**;127(Pt 6):1179-89 doi 10.1242/jcs.131227.

29. Varzavand A, Drake JM, Svensson RU, Herndon ME, Zhou B, Henry MD, *et al.* Integrin alpha3beta1 regulates tumor cell responses to stromal cells and can function to suppress prostate cancer metastatic colonization. Clin Exp Metastasis **2013**;30(4):541-52 doi 10.1007/s10585-012-9558-1.

30. Hu F, Zhao L, Wang Y, Ye H, Tang H, Zhou J. Integrated bioinformatics analysis shows integrin alpha 3 is a prognostic biomarker for pancreatic cancer. Open Med (Wars) **2022**;17(1):1935-43 doi 10.1515/med-2022-0606.

31. Idichi T, Seki N, Kurahara H, Fukuhisa H, Toda H, Shimonosono M, *et al.* Involvement of anti-tumor miR-124-3p and its targets in the pathogenesis of pancreatic ductal adenocarcinoma: direct regulation of ITGA3 and ITGB1 by miR-124-3p. Oncotarget **2018**;9(48):28849-65 doi 10.18632/oncotarget.25599.

32. Iwatate Y, Yokota H, Hoshino I, Ishige F, Kuwayama N, Itami M, *et al.* Transcriptomic analysis reveals high ITGB1 expression as a predictor for poor prognosis of pancreatic cancer. PLoS One **2022**;17(6):e0268630 doi 10.1371/journal.pone.0268630.

33. Jiao Y, Li Y, Liu S, Chen Q, Liu Y. ITGA3 serves as a diagnostic and prognostic biomarker for pancreatic cancer. Onco Targets Ther **2019**;12:4141-52 doi 10.2147/OTT.S201675.

34. Li J, Peng L, Chen Q, Ye Z, Zhao T, Hou S, *et al.* Integrin beta1 in Pancreatic Cancer: Expressions, Functions, and Clinical Implications. Cancers (Basel) **2022**;14(14) doi 10.3390/cancers14143377.

35. Lu Y, Hu J, Sun W, Li S, Deng S, Li M. MiR-29c inhibits cell growth, invasion, and migration of pancreatic cancer by targeting ITGB1. Onco Targets Ther **2016**;9:99-109 doi 10.2147/OTT.S92758.

36. Zhang W, Han S, Yuan Y, Xu M, Ding A, Li M. FTO Knockdown-Mediated Maturation of miR-383-5p Inhibits Malignant Advancement of Pancreatic Cancer by Targeting ITGA3. Biochem Genet **2024**;62(4):2652-66 doi 10.1007/s10528-023-10560-0.

37. Johnson PC, Gainor JF, Sullivan RJ, Longo DL, Chabner B. Immune Checkpoint Inhibitors - The Need for Innovation. N Engl J Med **2023**;388(16):1529-32 doi 10.1056/NEJMsb2300232.

38. Ju Y, Xu D, Liao MM, Sun Y, Bao WD, Yao F, *et al.* Barriers and opportunities in pancreatic cancer immunotherapy. NPJ Precis Oncol **2024**;8(1):199 doi 10.1038/s41698-024-00681-z.

39. Beatson R, Tajadura-Ortega V, Achkova D, Picco G, Tsourouktsoglou TD, Klausing S, *et al.* The mucin MUC1 modulates the tumor immunological microenvironment through engagement of the lectin Siglec-9. Nat Immunol **2016**;17(11):1273-81 doi 10.1038/ni.3552.

40. Hudak JE, Canham SM, Bertozzi CR. Glycocalyx engineering reveals a Siglec-based mechanism for NK cell immunoevasion. Nat Chem Biol **2014**;10(1):69-75 doi 10.1038/nchembio.1388.

41. Jandus C, Boligan KF, Chijioke O, Liu H, Dahlhaus M, Demoulins T, *et al.* Interactions between Siglec-7/9 receptors and ligands influence NK cell-dependent tumor immunosurveillance. J Clin Invest **2014**;124(4):1810-20 doi 10.1172/JCI65899.

42. Stanczak MA, Siddiqui SS, Trefny MP, Thommen DS, Boligan KF, von Gunten S, *et al.* Self-associated molecular patterns mediate cancer immune evasion by engaging Siglecs on T cells. J Clin Invest **2018**;128(11):4912-23 doi 10.1172/JCI120612.

43. Egan H, Treacy O, Lynch K, Leonard NA, O'Malley G, Reidy E, *et al.* Targeting stromal cell sialylation reverses T cell-mediated immunosuppression in the tumor microenvironment. Cell Rep **2023**;42(5):112475 doi 10.1016/j.celrep.2023.112475.

44. Mei Y, Wang X, Zhang J, Liu D, He J, Huang C, *et al.* Siglec-9 acts as an immune-checkpoint molecule on macrophages in glioblastoma, restricting T-cell priming and immunotherapy response. Nat Cancer **2023**;4(9):1273-91 doi 10.1038/s43018-023-00598-9.

45. Wang J, Manni M, Barenwaldt A, Wieboldt R, Kirchhammer N, Ivanek R, *et al.* Siglec Receptors Modulate Dendritic Cell Activation and Antigen Presentation to T Cells in Cancer. Front Cell Dev Biol **2022**;10:828916 doi 10.3389/fcell.2022.828916.

46. Varki A, Gagneux P. Multifarious roles of sialic acids in immunity. Annals of the New York Academy of Sciences **2012**;1253:16-36 doi 10.1111/j.1749-6632.2012.06517.x.

47. Su C, Wang H, Liu Y, Guo Q, Zhang L, Li J, *et al.* Adverse Effects of Anti-PD-1/PD-L1 Therapy in Non-small Cell Lung Cancer. Front Oncol **2020**;10:554313 doi 10.3389/fonc.2020.554313.

48. Chang L, Chen YJ, Fan CY, Tang CJ, Chen YH, Low PY, *et al.* Identification of Siglec Ligands Using a Proximity Labeling Method. J Proteome Res **2017**;16(10):3929-41 doi 10.1021/acs.jproteome.7b00625.

49. Crissey MAS, Versace A, Bhardwaj M, Jain V, Liu S, Singh A, *et al.* Divergent effects of acute and chronic PPT1 inhibition in melanoma. Autophagy **2024**:1-13 doi 10.1080/15548627.2024.2403152.

50. Cox J, Mann M. MaxQuant enables high peptide identification rates, individualized p.p.b.-range mass accuracies and proteome-wide protein quantification. Nat Biotechnol **2008**;26(12):1367-72 doi 10.1038/nbt.1511.

ACKNOWLEDGMENTS

M.A-M is supported by NIH grants (NIH R01AI165079, R01AA029859, R01DK123733, R01AG062383, and R01NS117458). M.A-M is also funded by the NIH-funded BEAT-HIV Martin Delaney Collaboratory to cure HIV-1 infection (1UM1Al126620). NIH R50CA221838 provided support to the Proteomics Facility at the Wistar Institute.

AUTHOR CONTRIBUTIONS

M.A.-M. conceived and designed the study. P.S. carried out the majority of the experiments. G.M. and S.A.B. performed the animal experiments. R.S. supervised and designed the animal experiments. J.C. and H.-Y.T. conducted the SPR and mass spectrometry analyses. K.M. consulted on the generation of the antibodies. H.T and R.Z interpreted the data. P.S. and M.A.-M. wrote the manuscript, and all authors edited it.

COMPETING INTERESTS STATEMENT

The authors have no competing interests.

FIGURE LEGENDS

Figure 1. PDAC cell lines expresses Siglec-10 ligands other than CD24. (a) Comparison of Siglec-10 and CD24 expression between normal tissues and pancreatic adenocarcinoma (PAAD) tissues from the TCGA dataset. Unpaired t tests. * = P<0.05. **(b)** A schematic representation of the glycan ligands of Siglec-10 on *N*-linked and *O*-linked glycans, along with the enzymes involved in their formation. **(c-d)** Expression levels of sialyltransferase enzymes responsible for Siglec-10 ligand formation compared between normal tissues and PAAD tissues in the TCGA dataset. Unpaired t tests. * = P<0.05. **(e)** Schematic overview of *in vitro* cancer cell killing experiments. Human monocyte-derived macrophages were differentiated into macrophages using M-CSF for three days, followed by M-CSF and IL-4 for an additional four days. PDAC cell lines were labeled with pHrodo Red dye and co-cultured with macrophages in the presence of either isotype control or CD24 antibody. Phagocytosis was monitored via live-cell imaging every hour, with total red area (μm^2/well) used as a measure of phagocytic activity. **(f)** (Top) Evaluation of anti-CD24 antibody (olive green bars) in enhancing macrophage-mediated phagocytosis of PDAC cells (AsPC-1, PANC-1, BxPC3, and MiaPaCa-2) compared to isotype control (gray bars). (Bottom) Time-course representation of phagocytosis in AsPC-1 and MiaPaCa-2 cells treated with anti-CD24 antibody (olive green) or isotype control (gray). Each symbol represents different donor/experiment. Ratio paired t-tests. **(g)** Flow cytometric analysis of Siglec-10 ligand and CD24 expression in MiaPaCa-2 cells. Siglec-10 ligands were detected using a recombinant Siglec-10-Fc chimeric protein and a secondary antibody (x-axis), and CD24 was detected using a specific antibody (y-axis). Cells binding Siglec-10 are highlighted (blue box), with subsets expressing CD24 (olive green box) or lacking CD24 expression (purple box). Similar analyses were performed for AsPC-1 and BxPC-3 cells. **(h)** Quantification of Siglec-10 ligand (blue bars) and CD24 (olive green bars) expression in PDAC cell lines by flow cytometry, presented as both the percentage of positive cells and median fluorescence intensity (MFI).

Figure 2. ITGA3 and ITGB1 are sialylated glycoprotein ligands of Siglec-10 glycoproteins on PDAC cells. (a) Experimental design for the pull-down of Siglec-10 ligands on PDAC cells. Recombinant Siglec-10 (as well as no-protein control or Siglec-5 control) Fc was allowed to bind its physiological ligands on the surface of PDAC cells, followed by an HRP-conjugated anti-Fc secondary antibody. In the presence of H□O□, HRP generated short-lived radicals that facilitated the transfer of biotin to proximal Siglec-10 ligands. Biotinylated Siglec-10 ligands were pulled down using streptavidin beads and identified by mass spectrometry. **(b)** A total of 4,044 proteins were identified, with enriched binding compared to a control using the anti-Fc antibody only without Siglec-10 protein. Of these, 110 proteins showed enrichment relative to a Siglec-5 control. Six proteins—CD47, CD59, CD73, ITGB6, ITGA3, and ITGB1—were significantly overexpressed in PAAD tissues compared to normal tissues in the TCGA dataset. **(c)** Response curves showing interactions between Siglec-10 and the six glycoproteins measured by surface plasmon resonance (SPR). Two concentrations (1000 nM, green; 100 nM, red) were tested for all glycoproteins, while ITGA3 was also tested at 300 nM (green) and 30 nM (red). **(d)** Binding of the SNA lectin (specific for sialic acid) to ITGA3 and ITGB1 recombinant glycoproteins was measured by a lectin array. Sialidase-treated glycoproteins (red bars) showed significantly reduced binding compared to untreated glycoproteins (blue bars). Unpaired t-tests were used for statistical analyses. **(e)** SPR response curves comparing the binding of intact (sialylated) ITGA3 and desialylated ITGA3 to immobilized Siglec-10. **(f)** SPR response curves comparing the binding of intact (sialylated) ITGB1 and desialylated ITGB1 to immobilized Siglec-10.

Figure 3. ITGA3 and ITGB1 are overexpressed in PDAC tissues and associated with poor survival in PDAC. (a) Flow cytometric analysis of ITGA3 expression on PDAC cell lines (HS766T, AsPC-1, and PANC-1) along the x-axis. **(b)** Comparative expression of ITGA3 in PAAD tissues versus normal tissues in the TCGA dataset. Unpaired t tests. * = $P<0.05$. **(c)** Flow cytometric analysis of ITGB1 expression on PDAC cell lines (HS766T, AsPC-1, and PANC-1) along the x-axis. **(d)** Comparative expression of ITGB1 in PAAD tissues versus normal tissues in the TCGA dataset. Unpaired t tests. * = $P<0.05$. **(e–g)** Survival analysis of pancreatic tumor patients in the TCGA dataset showing the correlation between **(e)** CD24, **(f)** ITGA3, and **(g)**

ITGB1 expression on overall survival. **(h)** Single-cell RNA-seq analysis of publicly available datasets using BBrowser software. Clusters representing distinct cell types were categorized into normal (blue clusters) and PDAC (orange clusters). **(i)** ITGA3 expression levels in epithelial cell clusters from normal tissues (blue bar) and PDAC tissues (orange bar). The intensity of red represents the expression of ITGA3, with darker shades indicating higher expression levels. Mann Whitney u test was used for statistical analysis. **(j)** Pathway analysis comparing ITGA3^{hi} and ITGA3^{low} epithelial cells in PDAC tissues to identify upregulated and downregulated pathways. **(k)** ITGB1 expression levels in epithelial cell clusters from normal tissues (blue bar) and PDAC tissues (orange bar). The intensity of red represents the expression of ITGB1, with darker shades indicating higher expression levels. Mann Whitney u test was used for statistical analysis.

Figure 4. ITGA3- and ITGB1-expressing PDAC cells evade macrophage-mediated phagocytosis. (a) Schematic representation of the experimental setup to enrich for ITGA3^{low} or ITGB1^{low} PDAC cells. Columns coated with anti-ITGA3 or anti-ITGB1 antibodies were used to isolate ITGA3^{low} or ITGB1^{low} cells (cells passing through the columns without binding), respectively. Cells passing through uncoated columns (expressing high levels of ITGA3 or ITGB1) were used as controls. **(b)** Representative flow cytometry analysis showing the expression of ITGA3 (left) or Siglec-10 ligands (right) expression levels on MIA PaCa-2 cells, depleted from ITGA3^{hi} cells (ITGA3^{low}) or not (control cells; Ctrl cells). **(c)** Schematic representation of the experimental setup to test the phagocytic capacity of monocyte-derived macrophages targeting control cells (enriched with ITGA3^{hi} cells) or ITGA3^{low} cells (n = 4–6). **(d-e)** Phagocytosis of control and ITGA3^{low} MIA PaCa-2 (c) or PANC1 (d) PDAC cells by macrophages from different donors. Top: Representative images where increased red indicates higher phagocytosis. Bottom left: Live imaging results (each symbol represents data from one donor). Bottom right: Area under the curve (AUC) data compiled from multiple donors. Statistical significance was assessed using ratio paired t-tests. **(f)** Schematic representation of the experimental setup to test the phagocytic capacity of monocyte-derived macrophages targeting control cells (enriched with ITGB1^{hi} cells) or ITGB1^{low} cells (n = 4–6). **(g-h)** Phagocytosis of control and ITGB1^{low} MIA PaCa-2 (f) or PANC1 (g) PDAC cells by macrophages from different

donors. Top: Representative images showing phagocytosis (increased red indicates higher phagocytosis). Bottom left: Live imaging results (each symbol represents data from one donor). Bottom right: AUC data compiled from multiple donors. Statistical significance was assessed using ratio paired t-tests.

Figure 5. Development of Siglec-10 blocking antibodies to enhance the phagocytosis of PDAC cells by macrophages *in vitro*. (a) Model illustrating the mechanism of Siglec-10-mediated inhibition of macrophage phagocytosis. Siglec-10 expressed on macrophages binds to its glycan ligands on PDAC cells, which are present on multiple proteins such as ITGA3, ITGB1, and CD24. This interaction induces inhibitory signaling in macrophages, suppressing phagocytosis (left panel). Blocking Siglec-10 with an antibody prevents inhibitory signaling, thereby enhancing macrophage phagocytic ability (right panel). **(b)** Screening of recombinant antibodies from the top clones for Siglec-10 binding using ELISA. Binding to immobilized Siglec-10 (blue) and Siglec-5 (gray) proteins is shown. **(c)** Flow cytometric analysis of clone selectivity, showing binding to CHO-K1 cells expressing either Siglec-10 (blue) or Siglec-5 (gray). **(d)** Area under the curve (AUC) analysis of an *in vitro* phagocytosis assay to screen the ability of Siglec-10 antibody clones, as well as the commercially available antibodies against CD24 and Siglec-10, to enhance the phagocytic activity of macrophages against AsPC-1 PDAC cells. **(e)** AUC analysis of the *in vitro* phagocytosis assay for the top-performing Siglec-10 antibody clone using macrophages differentiated from the monocytes of four donors. Statistical significance was determined using Friedman's ANOVA test. **(f)** Time-course analysis of the *in vitro* phagocytosis assay for the top Siglec-10 blocking antibody clone (68A11A1, blue) compared to the isotype control (gray). Results are based on n=4 independent experiments. **(g)** ELISA-based binding analysis of the 68A11A1 recombinant antibody to immobilized recombinant Siglec-10 and Siglec-5 proteins at different dilutions. **(h)** Evaluation of the ability of anti-CD24 or recombinant Siglec-10 antibody (clone 68A11A1) to enhance macrophage-mediated phagocytosis of several PDAC cell lines (AsPC-1, MIA PaCa-2, and PANC-1). Phagocytosis was normalized to the isotype control for each antibody and conducted using macrophages differentiated from monocytes of 5–8 healthy donors. Each symbol represents data from an individual donor, and statistical analyses were performed using ratio paired t-tests

compared to the isotype control. On the right, a representative image of the killing assays is shown (red indicates increased killing).

Figure 6. Blocking Siglec-10 interactions enhance macrophage-mediated phagocytosis and reduce PDAC tumor size *in vivo*. (a) Experimental design for subcutaneous tumor development and Siglec-10 antibody treatment. A total of 2 million AsPC-1 cells were subcutaneously injected into immunodeficient NSG mice. After 7 days, when tumors reached ~45 mm^3, mice were randomized into treatment groups. On the indicated days, approximately 3 million monocyte-derived macrophages were injected intravenously along with 200 µg of either isotype control or Siglec-10 antibody. Tumor size was measured on the specified days using a Vernier caliper. On the final day, tumors were excised for RNA-seq analysis. **(b)** Tumor volume was measured over time (x-axis) in mice treated with isotype control (pink dots) or Siglec-10 antibody (blue dots). Data represent n=10 mice per group. **(c–e)** Tumor assessments on day 31 after tumor induction and treatment: (c) tumor volume, (d) tumor weight, and (e) representative tumor images from mice treated with isotype control (grey dots) or Siglec-10 antibody (blue dots)**.** Data represent n=10 mice per group. Mann Whitney u test was used for statistical analysis. **(f–h)** Heatmaps showing differential gene expression in FACS-sorted human macrophages from tumors of subcutaneous PDAC-bearing mice treated with Siglec-10 antibody, highlighting: **(f)** immune activation pathways, **(g)** phagocytosis-related genes, and **(h)** metabolism-related genes. Red represents higher expression while blue represents lower expression.

SUPPLEMENTARY FIGURE LEGENDS

Supplementary Figure 1. Monocyte-derived macrophages express Siglec-10. A flow cytometry-based analysis of monocytes (top) and macrophages derived from monocytes (bottom) for Siglec-10 expression.

Supplementary Figure 2. ITGA3 and ITGAB1 highly expresses in PDAC cells. PDAC cells (MiaPaca-2 and BxPC3) were examined for their expression of (a) ITGA3 and (b) ITGB1 (x-axis) by flow cytometry.

Supplementary Figure 3. The expression of Siglec-10 and Siglec-10 ligand forming enzymes associated with the expression of ITGA3 and ITGB1. Spearman r correlation analysis in TCGA of (a) Siglec-10 with ITGA3, (b) ITGA3 with Siglec-10 ligand forming enzymes (ST3GAL1 and B3GNT3), (c) Siglec-10 with ITGB1, and (d) ITGB1 with Siglec-10 ligand forming enzymes (ST3GAL1 and B3GNT3).

Supplementary Figure 4. ITGA3 and ITGB1 highly expressed in PDAC epithelial cells. (a) ITGB1 high vs low pathway analysis for Fig (3). (b) Single cell RNA seq analysis from publicly available dataset (PMID:36781852) using BBrowser software. Each cluster representing different cell type. (c) ITGA3 expression examination on epithelial cell cluster in PDAC tissue. (d) Pathway analysis ITGA3 high vs low in epithelial cells from PDAC tissue from cluster represented in (c).

Supplementary Figure 5. Gating strategy for sorting the human tumor associated macrophages from mouse subcutaneous tumor. Single cell suspension from mouse subcutaneous tumor was used to obtain human monocytes derived macrophages injected 12hr intravenously for RNA seq analysis. Mouse BV711-CD45^{-} and Human APC-CD45^{+} cells were sorted for RNA seq analysis.

SUPPLEMENTARY TABLES

Supplementary Table 1. Sequences of the monoclonal antibodies against Siglec-10

Figure 1

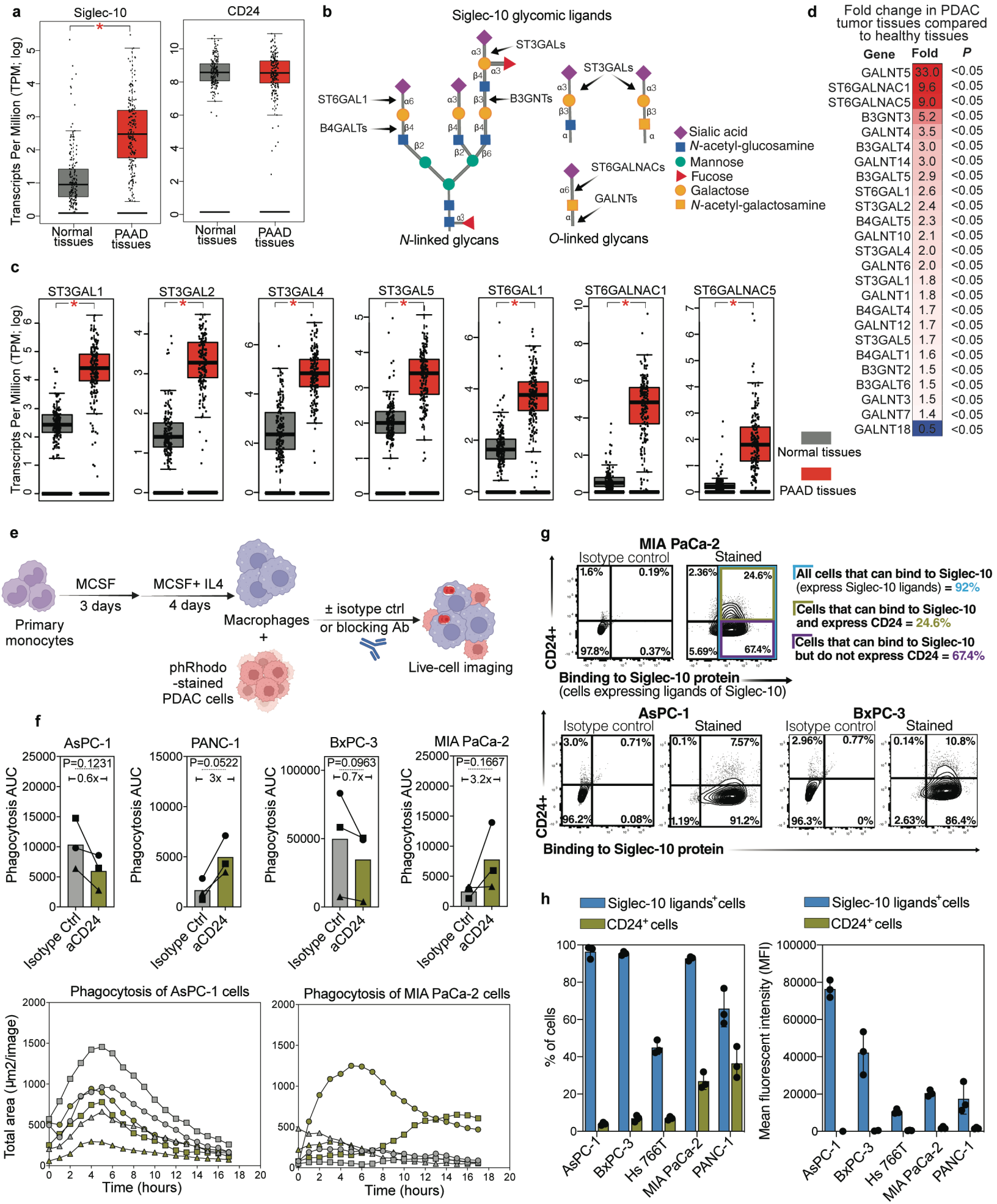
a
Siglec-10
CD24
Transcripts Per Million (TPM; log)
Normal tissues
PAAD tissues
b
Siglec-10 glycomic ligands
ST3GALs
ST6GAL1
B4GALTs
B3GNTs
ST6GALNACs
GALNTs
N-linked glycans
O-linked glycans
Sialic acid
N-acetyl-glucosamine
Mannose
Fucose
Galactose
N-acetyl-galactosamine
c
ST3GAL1
ST3GAL2
ST3GAL4
ST3GAL5
ST6GAL1
ST6GALNAC1
ST6GALNAC5
Normal tissues
PAAD tissues
d
Fold change in PDAC tumor tissues compared to healthy tissues
Gene Fold P
GALNT5 33.0 <0.05
ST6GALNAC1 9.6 <0.05
ST6GALNAC5 9.0 <0.05
B3GNT3 5.2 <0.05
GALNT4 3.5 <0.05
B3GALT4 3.0 <0.05
GALNT14 3.0 <0.05
B3GALT5 2.9 <0.05
ST6GAL1 2.6 <0.05
ST3GAL2 2.4 <0.05
B4GALT5 2.3 <0.05
GALNT10 2.1 <0.05
ST3GAL4 2.0 <0.05
GALNT6 2.0 <0.05
ST3GAL1 1.8 <0.05
GALNT1 1.8 <0.05
B4GALT4 1.7 <0.05
GALNT12 1.7 <0.05
ST3GAL5 1.7 <0.05
B4GALT1 1.6 <0.05
B3GNT2 1.5 <0.05
B3GALT6 1.5 <0.05
GALNT3 1.5 <0.05
GALNT7 1.4 <0.05
GALNT18 0.5 <0.05
e
Primary monocytes
MCSF
3 days
MCSF+ IL4
4 days
Macrophages
+
phRhodo -stained PDAC cells
± isotype ctrl or blocking Ab
Live-cell imaging
f
AsPC-1
PANC-1
BxPC-3
MIA PaCa-2
Phagocytosis AUC
P=0.1231
0.6x
P=0.0522
3x
P=0.0963
0.7x
P=0.1667
3.2x
Isotype Ctrl
aCD24
Phagocytosis of AsPC-1 cells
Phagocytosis of MIA PaCa-2 cells
Total area (µm2/image)
Time (hours)
g
MIA PaCa-2
Isotype control
Stained
CD24+
1.6%
0.19%
97.8%
0.37%
2.36%
24.6%
5.69%
67.4%
All cells that can bind to Siglec-10 (express Siglec-10 ligands) = 92%
Cells that can bind to Siglec-10 and express CD24 = 24.6%
Cells that can bind to Siglec-10 but do not express CD24 = 67.4%
Binding to Siglec-10 protein
(cells expressing ligands of Siglec-10)
AsPC-1
BxPC-3
3.0%
0.71%
96.2%
0.08%
0.1%
7.57%
1.19%
91.2%
2.96%
0.77%
96.3%
0%
0.14%
10.8%
2.63%
86.4%
Binding to Siglec-10 protein
h
Siglec-10 ligands+cells
CD24+ cells
% of cells
Mean fluorescent intensity (MFI)
AsPC-1
BxPC-3
Hs 766T
MIA PaCa-2
PANC-1

Figure 2

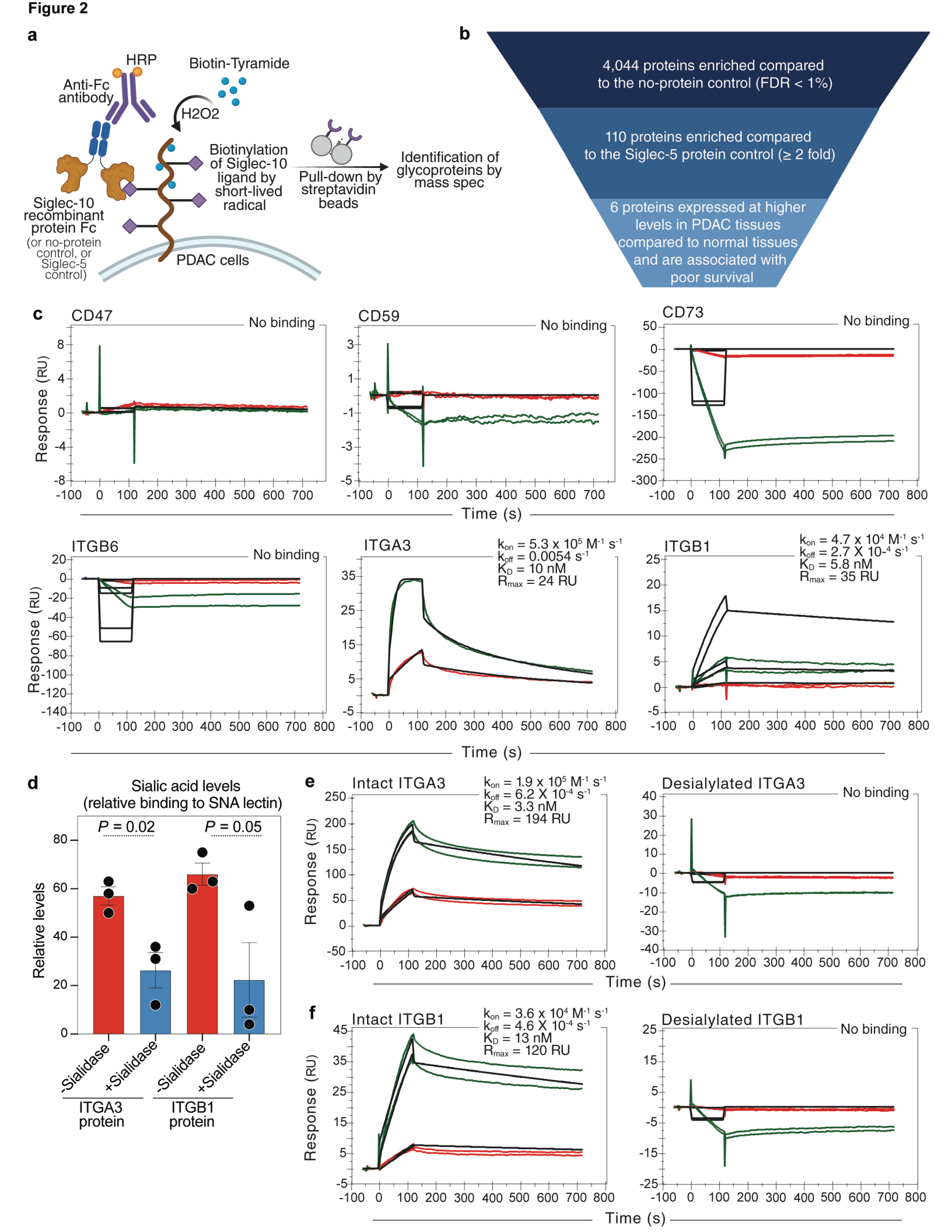
a
HRP
Biotin-Tyramide
Anti-Fc antibody
H2O2
Biotinylation of Siglec-10 ligand by short-lived radical
Pull-down by streptavidin beads
Identification of glycoproteins by mass spec
Siglec-10 recombinant protein Fc
(or no-protein control, or Siglec-5 control)
PDAC cells
b
4,044 proteins enriched compared to the no-protein control (FDR < 1%)
110 proteins enriched compared to the Siglec-5 protein control (≥ 2 fold)
6 proteins expressed at higher levels in PDAC tissues compared to normal tissues and are associated with poor survival
c
CD47
No binding
CD59
No binding
CD73
No binding
Response (RU)
Time (s)
ITGB6
No binding
ITGA3
k_{on} = 5.3 x 10^5 M^{-1} s^{-1}
k_{off} = 0.0054 s^{-1}
K_D = 10 nM
R_{max} = 24 RU
ITGB1
k_{on} = 4.7 x 10^4 M^{-1} s^{-1}
k_{off} = 2.7 X 10^{-4} s^{-1}
K_D = 5.8 nM
R_{max} = 35 RU
d
Sialic acid levels
(relative binding to SNA lectin)
P = 0.02
P = 0.05
Relative levels
-Sialidase
+Sialidase
-Sialidase
+Sialidase
ITGA3 protein
ITGB1 protein
e
Intact ITGA3
k_{on} = 1.9 x 10^5 M^{-1} s^{-1}
k_{off} = 6.2 X 10^{-4} s^{-1}
K_D = 3.3 nM
R_{max} = 194 RU
Desialylated ITGA3
No binding
f
Intact ITGB1
k_{on} = 3.6 x 10^4 M^{-1} s^{-1}
k_{off} = 4.6 X 10^{-4} s^{-1}
K_D = 13 nM
R_{max} = 120 RU
Desialylated ITGB1
No binding

Figure 3

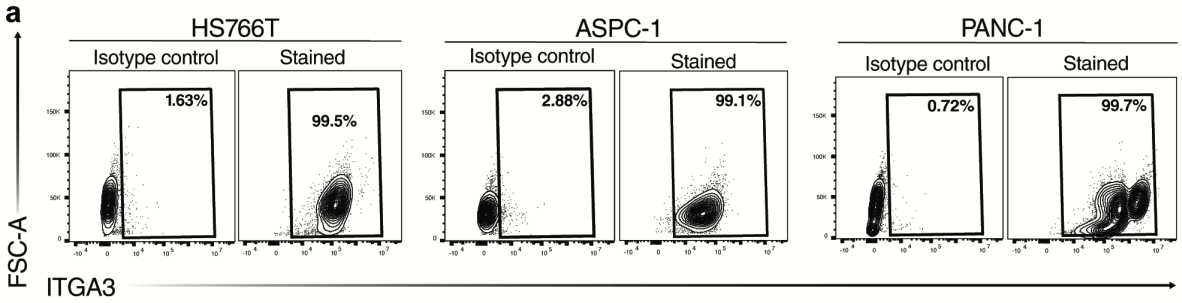
a
HS766T
ASPC-1
PANC-1
Isotype control
Stained
1.63%
99.5%
2.88%
99.1%
0.72%
99.7%
FSC-A
ITGA3

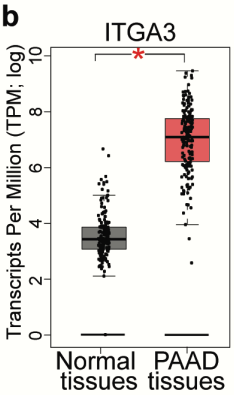
b
ITGA3
Transcripts Per Million (TPM; log)
Normal tissues
PAAD tissues

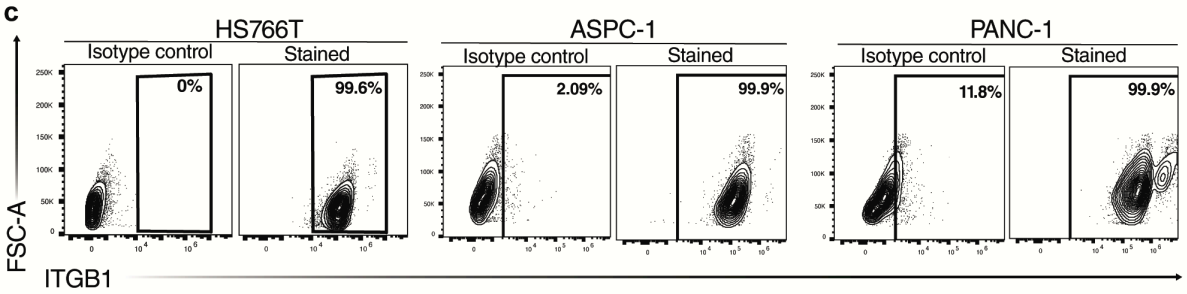
c
HS766T
ASPC-1
PANC-1
Isotype control
Stained
0%
99.6%
2.09%
99.9%
11.8%
99.9%
FSC-A
ITGB1

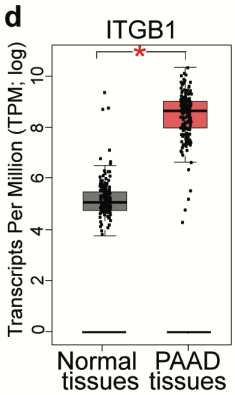
d
ITGB1
Transcripts Per Million (TPM; log)
Normal tissues
PAAD tissues

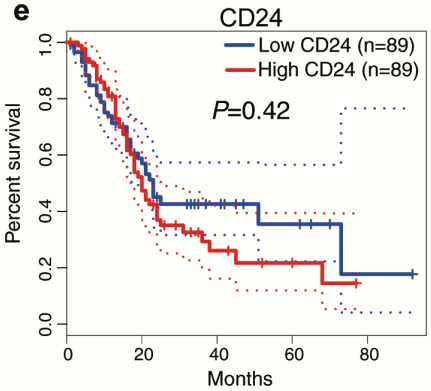
e
CD24
Low CD24 (n=89)
High CD24 (n=89)
P=0.42
Percent survival
Months

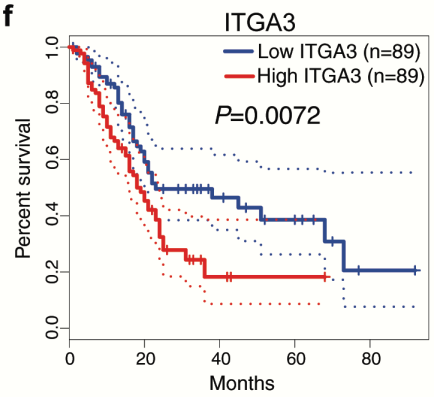
f
ITGA3
Low ITGA3 (n=89)
High ITGA3 (n=89)
P=0.0072
Percent survival
Months

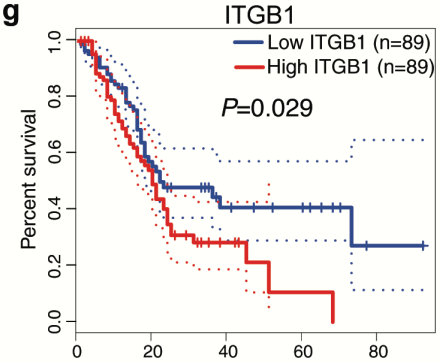
g
ITGB1
Low ITGB1 (n=89)
High ITGB1 (n=89)
P=0.029
Percent survival
Months

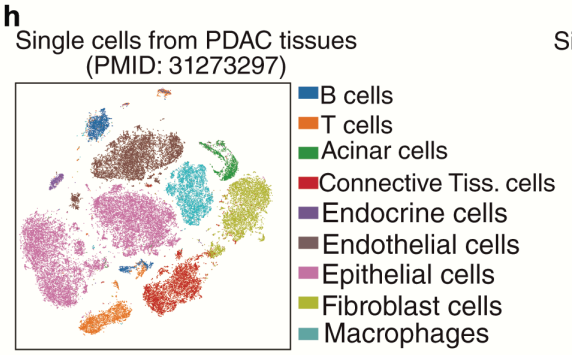
h
Single cells from PDAC tissues
(PMID: 31273297)
B cells
T cells
Acinar cells
Connective Tiss. cells
Endocrine cells
Endothelial cells
Epithelial cells
Fibroblast cells
Macrophages

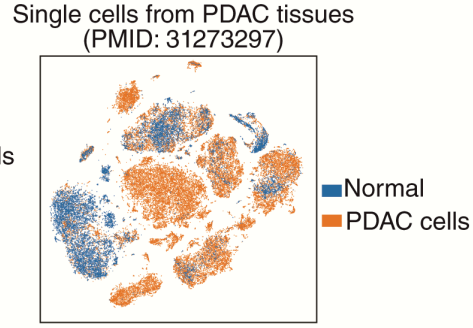
Single cells from PDAC tissues
(PMID: 31273297)
Normal
PDAC cells

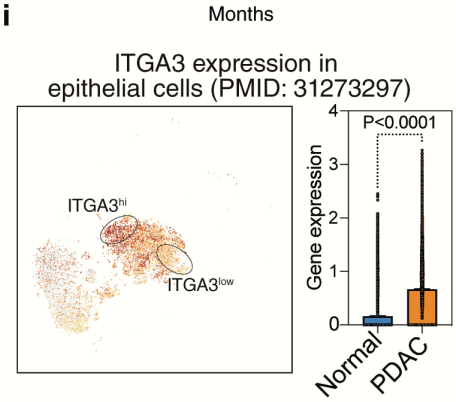
i
ITGA3 expression in
epithelial cells (PMID: 31273297)
ITGA3hi
ITGA3low
P<0.0001
Gene expression
Normal
PDAC

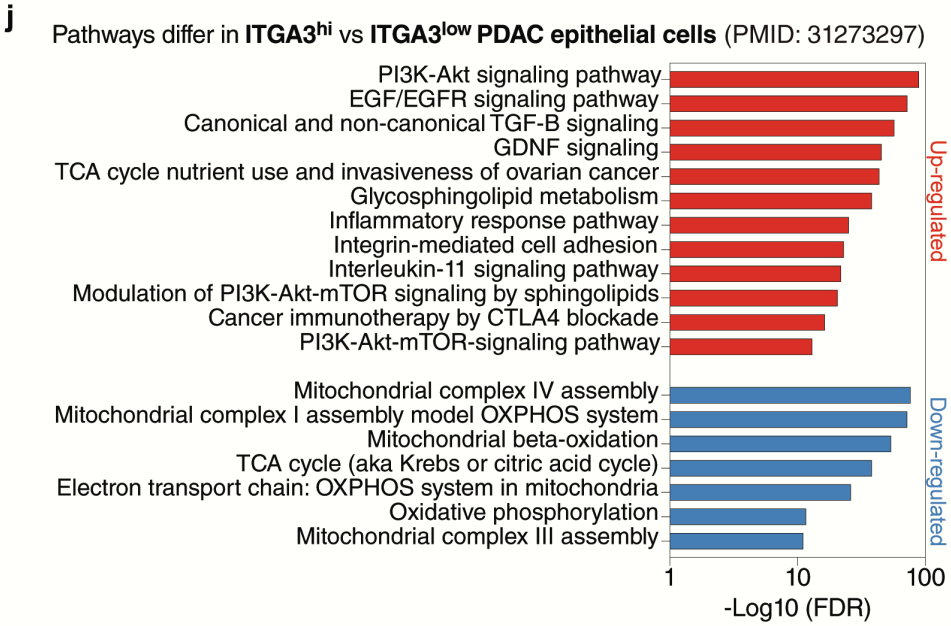
j
Pathways differ in ITGA3hi vs ITGA3low PDAC epithelial cells (PMID: 31273297)
PI3K-Akt signaling pathway
EGF/EGFR signaling pathway
Canonical and non-canonical TGF-B signaling
GDNF signaling
TCA cycle nutrient use and invasiveness of ovarian cancer
Glycosphingolipid metabolism
Inflammatory response pathway
Integrin-mediated cell adhesion
Interleukin-11 signaling pathway
Modulation of PI3K-Akt-mTOR signaling by sphingolipids
Cancer immunotherapy by CTLA4 blockade
PI3K-Akt-mTOR-signaling pathway
Mitochondrial complex IV assembly
Mitochondrial complex I assembly model OXPHOS system
Mitochondrial beta-oxidation
TCA cycle (aka Krebs or citric acid cycle)
Electron transport chain: OXPHOS system in mitochondria
Oxidative phosphorylation
Mitochondrial complex III assembly
Up-regulated
Down-regulated
-Log10 (FDR)

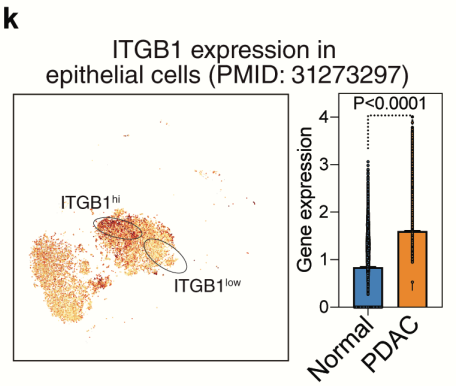
k
ITGB1 expression in
epithelial cells (PMID: 31273297)
ITGB1hi
ITGB1low
P<0.0001
Gene expression
Normal
PDAC

Figure 4

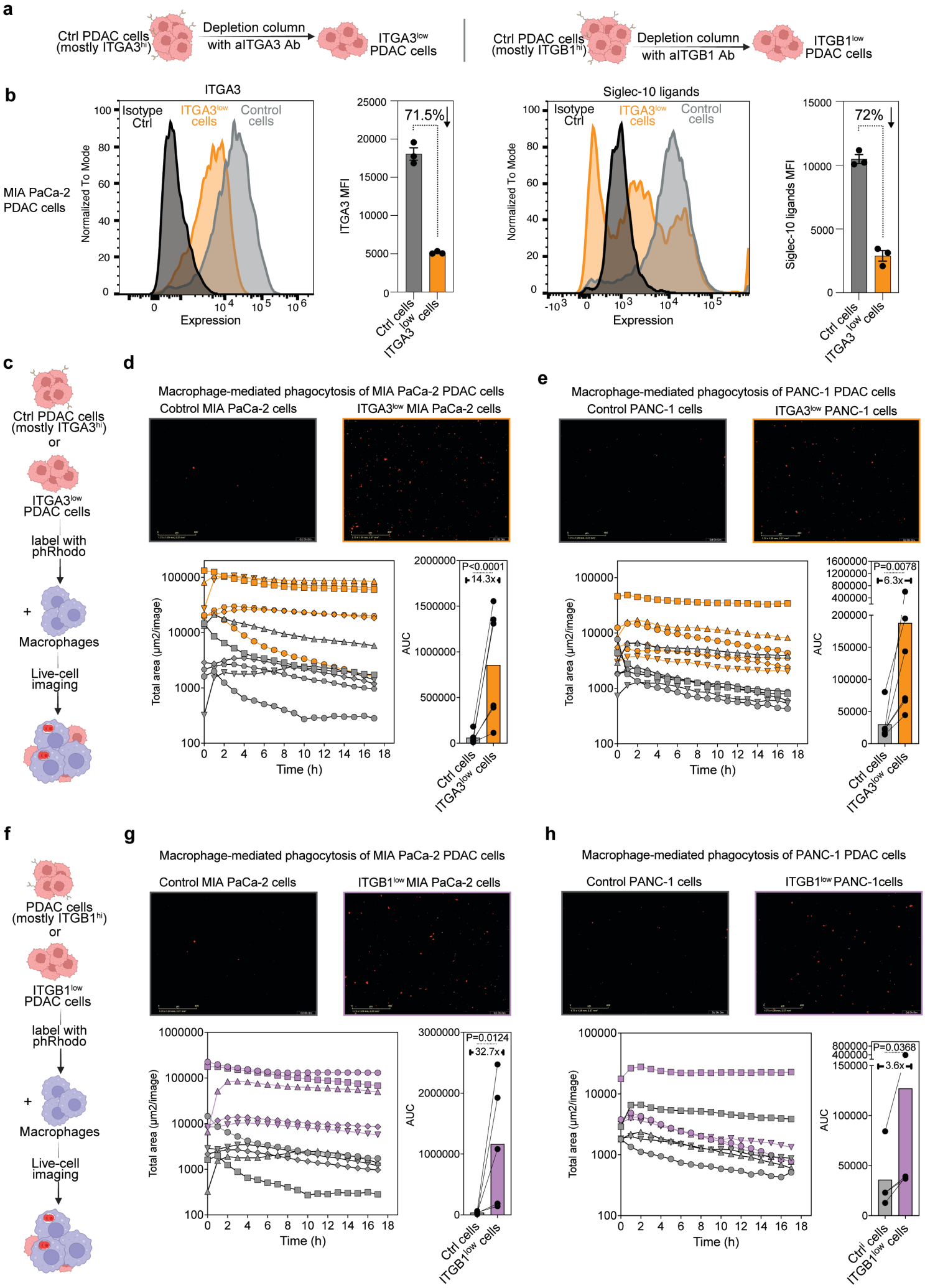
a
Ctrl PDAC cells (mostly ITGA3hi)
Depletion column with aITGA3 Ab
ITGA3low PDAC cells
Ctrl PDAC cells (mostly ITGB1hi)
Depletion column with aITGB1 Ab
ITGB1low PDAC cells
b
MIA PaCa-2 PDAC cells
ITGA3
Isotype Ctrl
ITGA3low cells
Control cells
Normalized To Mode
Expression
ITGA3 MFI
71.5%
Ctrl cells
ITGA3low cells
Siglec-10 ligands
Siglec-10 ligands MFI
72%
c
Ctrl PDAC cells (mostly ITGA3hi)
or
ITGA3low PDAC cells
label with phRhodo
+
Macrophages
Live-cell imaging
d
Macrophage-mediated phagocytosis of MIA PaCa-2 PDAC cells
Cobtrol MIA PaCa-2 cells
ITGA3low MIA PaCa-2 cells
Total area (µm2/image)
Time (h)
AUC
P<0.0001
14.3x
e
Macrophage-mediated phagocytosis of PANC-1 PDAC cells
Control PANC-1 cells
ITGA3low PANC-1 cells
P=0.0078
6.3x
f
PDAC cells (mostly ITGB1hi)
or
ITGB1low PDAC cells
label with phRhodo
+
Macrophages
Live-cell imaging
g
Macrophage-mediated phagocytosis of MIA PaCa-2 PDAC cells
Control MIA PaCa-2 cells
ITGB1low MIA PaCa-2 cells
P=0.0124
32.7x
ITGB1low cells
h
Macrophage-mediated phagocytosis of PANC-1 PDAC cells
Control PANC-1 cells
ITGB1low PANC-1cells
P=0.0368
3.6x

Figure 5

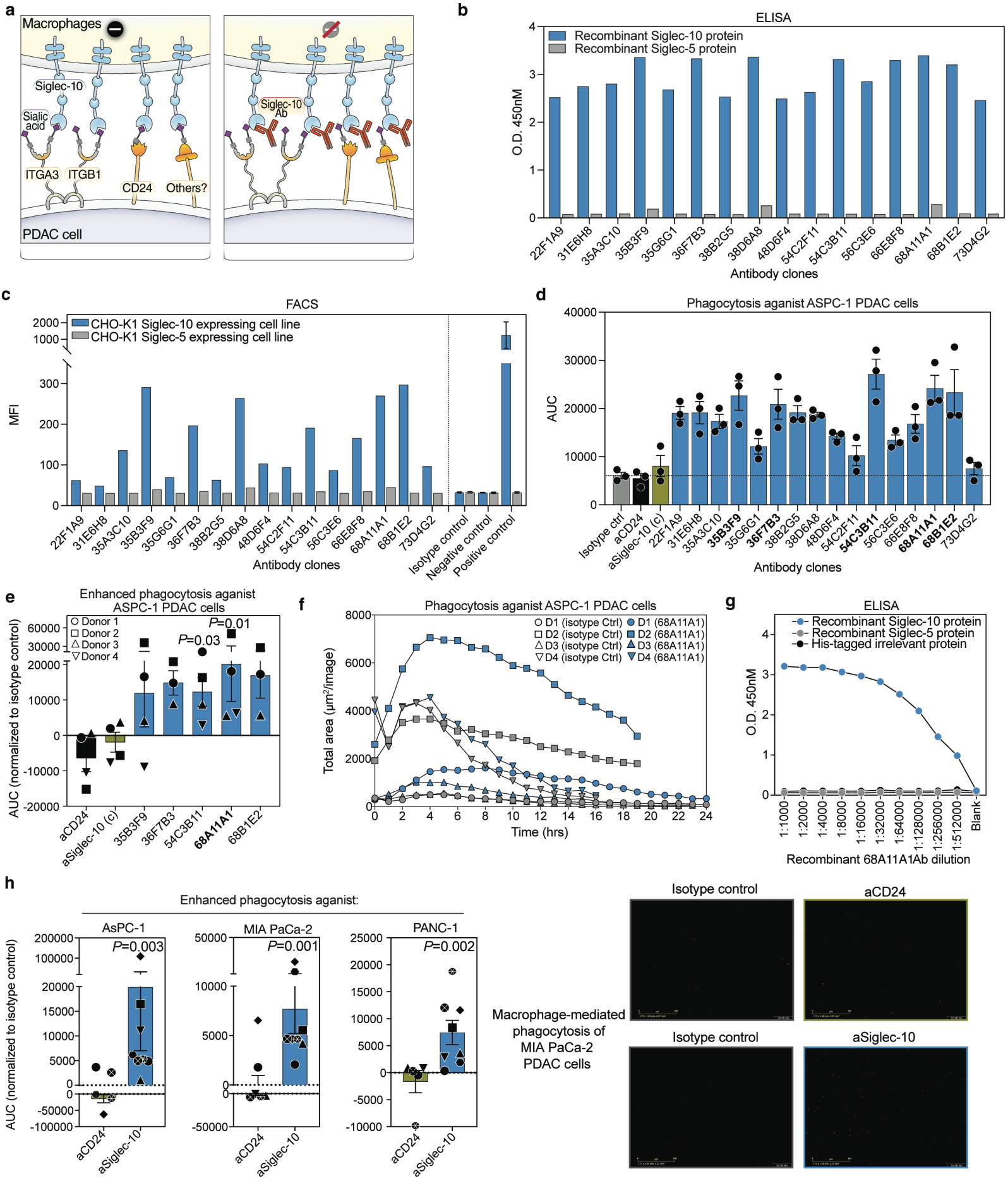
a
Macrophages
Siglec-10
Sialic acid
ITGA3
ITGB1
CD24
Others?
PDAC cell
Siglec-10 Ab
b
ELISA
Recombinant Siglec-10 protein
Recombinant Siglec-5 protein
O.D. 450nM
22F1A9
31E6H8
35A3C10
35B3F9
35G6G1
36F7B3
38B2G5
38D6A8
48D6F4
54C2F11
54C3B11
56C3E6
66E8F8
68A11A1
68B1E2
73D4G2
Antibody clones
c
FACS
CHO-K1 Siglec-10 expressing cell line
CHO-K1 Siglec-5 expressing cell line
MFI
Isotype control
Negative control
Positive control
Antibody clones
d
Phagocytosis aganist ASPC-1 PDAC cells
AUC
Isotype ctrl
aCD24
aSiglec-10 (c)
Antibody clones
e
Enhanced phagocytosis aganist ASPC-1 PDAC cells
Donor 1
Donor 2
Donor 3
Donor 4
P=0.01
P=0.03
AUC (normalized to isotype control)
aCD24
aSiglec-10 (c)
35B3F9
36F7B3
54C3B11
68A11A1
68B1E2
f
Phagocytosis aganist ASPC-1 PDAC cells
D1 (isotype Ctrl)
D2 (isotype Ctrl)
D3 (isotype Ctrl)
D4 (isotype Ctrl)
D1 (68A11A1)
D2 (68A11A1)
D3 (68A11A1)
D4 (68A11A1)
Total area (μm²/image)
Time (hrs)
g
ELISA
Recombinant Siglec-10 protein
Recombinant Siglec-5 protein
His-tagged irrelevant protein
O.D. 450nM
1:1000
1:2000
1:4000
1:8000
1:16000
1:32000
1:64000
1:128000
1:256000
1:512000
Blank
Recombinant 68A11A1Ab dilution
h
Enhanced phagocytosis aganist:
AsPC-1
MIA PaCa-2
PANC-1
P=0.003
P=0.001
P=0.002
AUC (normalized to isotype control)
aCD24
aSiglec-10
Macrophage-mediated phagocytosis of MIA PaCa-2 PDAC cells
Isotype control
aCD24
Isotype control
aSiglec-10

Figure 6

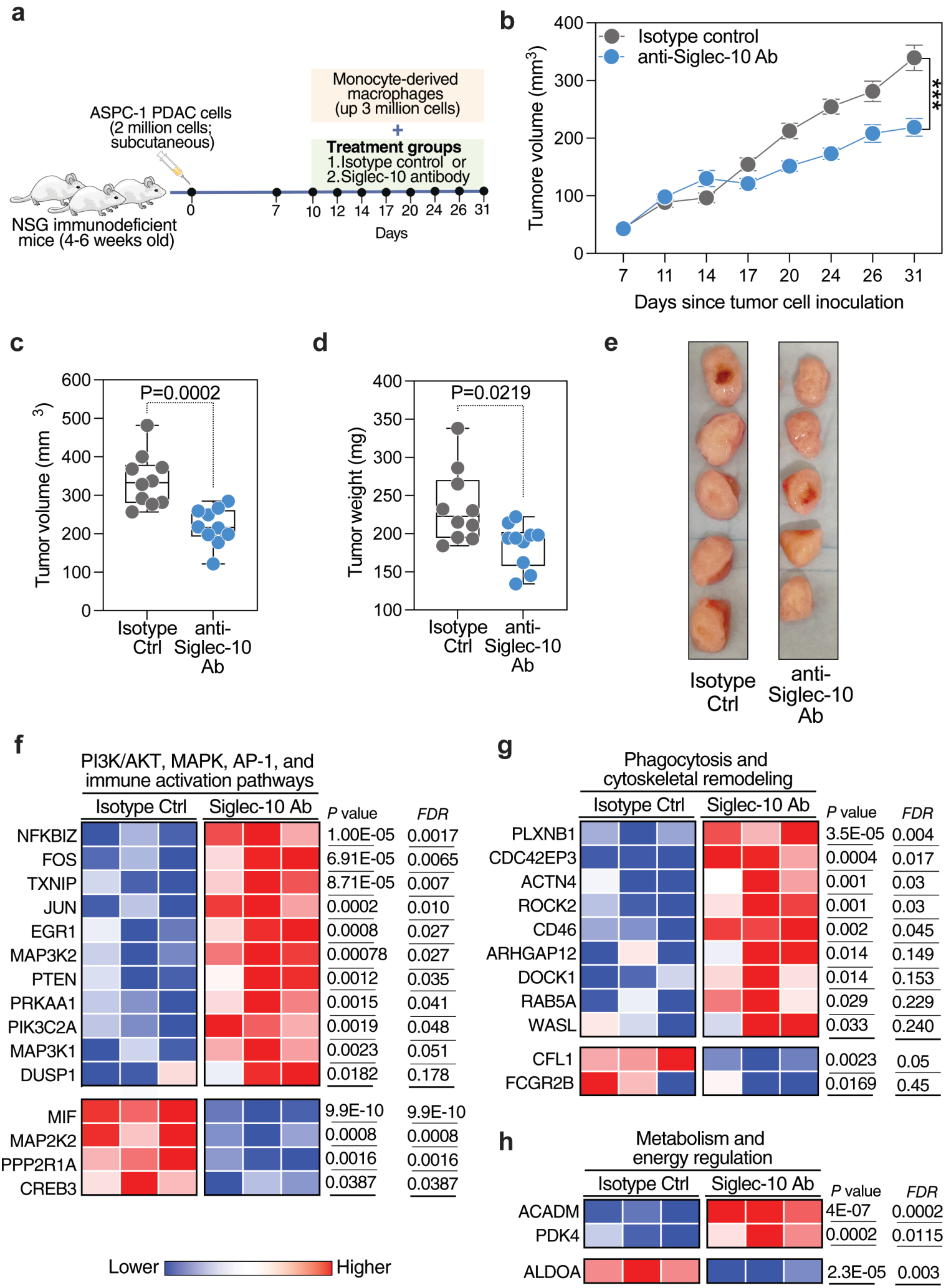
a
ASPC-1 PDAC cells
(2 million cells;
subcutaneous)
NSG immunodeficient
mice (4-6 weeks old)
Monocyte-derived
macrophages
(up 3 million cells)
+
Treatment groups
1.Isotype control or
2.Siglec-10 antibody
0 7 10 12 14 17 20 24 26 31
Days
b
Isotype control
anti-Siglec-10 Ab
Tumore volume (mm3)
400
300
200
100
0
7 11 14 17 20 24 26 31
Days since tumor cell inoculation
***
c
P=0.0002
Tumor volume (mm 3)
600
500
400
300
200
100
0
Isotype Ctrl
anti-Siglec-10 Ab
d
P=0.0219
Tumor weight (mg)
400
350
300
250
200
150
100
Isotype Ctrl
anti-Siglec-10 Ab
e
Isotype Ctrl
anti-Siglec-10 Ab
f
PI3K/AKT, MAPK, AP-1, and
immune activation pathways
Isotype Ctrl
Siglec-10 Ab
P value
FDR
NFKBIZ 1.00E-05 0.0017
FOS 6.91E-05 0.0065
TXNIP 8.71E-05 0.007
JUN 0.0002 0.010
EGR1 0.0008 0.027
MAP3K2 0.00078 0.027
PTEN 0.0012 0.035
PRKAA1 0.0015 0.041
PIK3C2A 0.0019 0.048
MAP3K1 0.0023 0.051
DUSP1 0.0182 0.178
MIF 9.9E-10 9.9E-10
MAP2K2 0.0008 0.0008
PPP2R1A 0.0016 0.0016
CREB3 0.0387 0.0387
Lower
Higher
g
Phagocytosis and
cytoskeletal remodeling
Isotype Ctrl
Siglec-10 Ab
P value
FDR
PLXNB1 3.5E-05 0.004
CDC42EP3 0.0004 0.017
ACTN4 0.001 0.03
ROCK2 0.001 0.03
CD46 0.002 0.045
ARHGAP12 0.014 0.149
DOCK1 0.014 0.153
RAB5A 0.029 0.229
WASL 0.033 0.240
CFL1 0.0023 0.05
FCGR2B 0.0169 0.45
h
Metabolism and
energy regulation
Isotype Ctrl
Siglec-10 Ab
P value
FDR
ACADM 4E-07 0.0002
PDK4 0.0002 0.0115
ALDOA 2.3E-05 0.003